



Journal of Geophysical Research: Space Physics

RESEARCH ARTICLE

10.1029/2018JA025225

Kev Points:

- The interval of the magnetic cloud is identified by means of the heliospheric current sheet, which happens to be in the ambient region
- The nature of the studied discontinuities is verified through multiple spacecraft observations
- A novel method to evaluate the uncertainties of interplanetary tangential discontinuities is provided

Correspondence to:

Y. H. Yang, yhyang@jupiter.ss.ncu.edu.tw

Citation:

Lin, P. H., Yang, Y. H., Chao, J. K., Feng, H. Q., & Liu, J. Y. (2018). Understanding magnetic cloud structure from shock/discontinuity analysis. *Journal of Geophysical Research: Space Physics*, 123. https://doi.org/10.1029/2018JA025225

Received 11 JAN 2018 Accepted 21 JUL 2018 Accepted article online 27 JUL 2018

Understanding Magnetic Cloud Structure From Shock/Discontinuity Analysis

P. H. Lin^{1,2}, Y. H. Yang², J. K. Chao², H. Q. Feng³, and J. Y. Liu²

¹Institute for Space-Earth Environmental Research, Nagoya University, Nagoya, Japan, ²Institute of Space Science, National Central University, Taoyuan, Taiwan, ³Institute of Space Physics, Luoyang Normal University, Luoyang, China

Abstract We reexamine the magnetic cloud (MC) event during the period of 21–23 May 2007. In this event, the axis of the MC has a high inclination to the ecliptic plane and the heliospheric current sheet happens to be on the ecliptic plane. Therefore, we can use the feature of zero north-south component of interplanetary magnetic field to identify the MC boundaries. Inside the MC, there is an enhanced pressure/density region enclosed by two discontinuities. We verified these discontinuities through multiple spacecraft in situ observations. The front one is a forward fast shock, which is a quasi-perpendicular shock at STEREO B but a quasi-parallel shock at Wind location. The discontinuity at the rear part of the enhanced pressure region resembles a reverse slow shock. However, we verify it is a tangential discontinuity (TD) using multispacecraft observations. Furthermore, we analyze the successive TDs inside the MC based on the TD signature of no normal magnetic field component to estimate the magnetic field morphology along the spacecraft trajectories. A novel method to evaluate the uncertainties of those TDs in this study has been given. It is found that the errors of the TD normal are much smaller than that calculated by conventional methods.

1. Introduction

Interplanetary coronal mass ejections (ICMEs) are the manifestations of coronal mass ejections (CMEs) in the interplanetary space. A typical structure of ICME consists of a leading shock, a transiting sheath, and a main body (Gosling et al., 1975; Kilpua et al., 2017; Sheeley Jr et al., 1980). The ICME can be further classified into an ejecta or a magnetic cloud (MC) depending on the magnetic field structure of the main body (Rouillard, 2011). According to Burlaga et al. (1981), a MC is characterized as (i) the smooth rotation of magnetic field during an interval of about one day, (ii) the stronger magnetic field than ambient solar wind, and (iii) the lower proton temperature and density compared to the surrounding plasma. The signature of smooth field rotation across an MC, indicating the helical magnetic fields wrapping around a central axis, is described as a magnetic flux rope. The feature of stronger magnetic field together with lower plasma density and temperature correspond to the smaller plasma beta inside an MC. Besides the large-scale MCs, some MCs are found to have smaller size lasting few hours (Crooker et al., 1996; Feng et al., 2007; Feng, Wu, et al., 2008; Moldwin et al., 2000; Yu et al., 2014). Parts of these small-scale MCs have different origin and mechanism from the large-scale MCs and thus excluded in this study.

Multispacecraft in situ observations provide a good opportunity to understand the magnetic field topology and the evolution of MCs. In combination with the near-Earth measurements (e.g., IMP 8, Wind, ACE, and STEREO spacecraft) and the measurements other than 1 AU (e.g., Helios, MESSENGER, Ulysses, and Voyager spacecraft), the radial variations in the interplanetary space of MC properties as well as the global dynamics of MCs are investigated extensively (e.g., Bothmer & Schwenn, 1998; Burlaga et al., 1990, 2001; Du et al., 2007; Good et al., 2015; Leitner et al., 2007; Liu et al., 2006; Nakwacki et al., 2011; Riley et al., 2003; Rodriguez et al., 2008; Skoug et al., 2000). It is common that MCs undergo expansion when propagating in heliosphere. The radial expansion of ICMEs was found to slow down beyond 1 AU and to maintain a constant width beyond 15 AU (Jian et al., 2008; Richardson et al., 2006; Von Steiger & Richardson, 2006). Moreover, owing to the launch of STEREO spacecraft (Kaiser et al., 2008), multipoint observations at different longitudinal locations around 1 AU can be utilized to examine the MC flux rope structure and field properties at different segments of the flux rope (e.g., Farrugia et al., 2011; Kilpua et al., 2009; Möstl, Earrugia, Miklenic, et al., 2009; Möstl et al., 2012; Ruffenach et al., 2012).

The boundaries of MCs can be identified by several signatures, such as the decrease of plasma β , temperature, and density (Burlaga et al., 1981), the bidirectional streaming of superthermal electrons (Gosling et al.,

©2018. American Geophysical Union. All Rights Reserved.

1987), or the structure of tangential discontinuity (TD; Feng et al., 2006). Wei et al. (2003) suggested that the MC boundaries usually display the properties of a reconnection layer. Identifying MC boundaries correctly is important not only because it is related to the solar eruptive events or the interaction with ambient solar wind but also because the MC-associated shock/discontinuity structures or the southward magnetic fields can affect the geomagnetic environment dramatically. However, it is difficult to obtain consistent results between different definitions, especially for the rear boundary. Many different approaches have been performed to reconstruct the magnetic field pattern on the MC cross section, such as the force-free field modeling (e.g., Burlaga, 1988; Goldstein, 1983; Lepping et al., 1990), the velocity-modified flux rope model (Wang et al., 2015), the minimum variance analysis (e.g., Lepping et al., 1990), the non-force-free field modeling (e.g., Hidalgo, 2002; Mulligan & Russell, 2001), and the Grad-Shafranov (GS) reconstruction (e.g., Hu & Sonnerup, 2002). It is suggested that the cross-section shape of an MC can be deformed into oblate instead of a circular shape when interacting with ambient solar wind structures (e.g., Démoulin et al., 2013; Farrugia et al., 1995; Liu et al., 2006; Mulligan & Russell, 2001; Owens, 2006; Riley et al., 2003; Wang et al., 2018). Note that either the different approaches with the same front and rear boundaries or the usage of different boundary selections in the same approach can produce different cross-section shapes. The comparison of various models can be found in Riley et al. (2004) and Al-Haddad et al. (2013).

In addition, some specific structures such as discontinuities, shocks, and pressure pulses are reported to appear inside MCs. Previous works mainly focus on the statistical properties of these internal structures or to study their possible causes through the interaction with ambient solar wind (e.g., Collier et al., 2007; Lepping et al., 2006; Tsurutani & Gonzalez, 1997; Wang et al., 2003), but rarely discuss their connections with the whole MC structure. In this study, we propose that we can deduce the portions of magnetic field morphology on the MC cross section along the spacecraft trajectories from the internal TDs of the studied MC. Theoretically, a TD is characterized as the boundary separating different magnetic field and plasma environments at both sides with no normal plasma flow and no normal magnetic field component across the discontinuity surface. And the total pressure of thermal plus magnetic field remains invariant across a TD. The helical magnetic field configuration inside an MC, as described by the force-free flux-rope model (Goldstein, 1983), indicates the feature of no radial magnetic field component. It means that an MC taken as a flux rope is composed of a series of specific structures surrounding the MC center axis with no magnetic field across these structures. Therefore, according to the magnetic flux rope model, there should be multiple cylindrical TD planes wrapping around the central axis of an MC.

We reexamine the MC event occurred during 21–23 May 2007 in this study. This MC is likely to have an axis highly inclined to the ecliptic plane around 1 AU and was passaged by the Wind, ACE, and STEREO spacecraft. Based on the analysis of magnetic field topology on the MC cross section, several studies suggest that STEREO B transited the MC central region but Wind encountered the east side of the MC (Hidalgo, 2013; Kilpua et al., 2009; Kilpua et al., 2011; Liu et al., 2008; Möstl, Farrugia, Miklenic, et al., 2009). STEREO B and ACE observed the feature of bidirectional suprathermal electrons within the MC (Chollet et al., 2010; Kilpua et al., 2009). The solar origin of this MC event was reported to be associated with a CME and prominence eruptions (Kilpua et al., 2009; Möstl, Farrugia, Miklenic, et al., 2009). Here we perform the detailed discontinuity/shock analysis by proposing new views of the MC rear boundary and the discontinuity/shock uncertainty estimations. We also suggest the possible passages of spacecraft through the MC via the analysis of internal TDs.

2. Identification the Major Discontinuities of the MC

Figure 1 shows the averaged positions of STEREO and Wind spacecraft in GSE coordinate on 22 May 2007, where the STEREO B locates at $(x, y, z)_{\rm GSE} = (-1,056, 1,345, -126)$ R_E, Wind locates at $(x, y, z)_{\rm GSE} = (239, 90, 15)$ R_E, and STEREO A locates at $(x, y, z)_{\rm GSE} = (1,363, -2,344, 26)$ R_E. It is thought that STEREO A only passed through the flank of the studied MC due to the unclear magnetic field rotation in STEREO A observations (Kilpua et al., 2009; Liu et al., 2008; Möstl, Farrugia, Miklenic, et al., 2009). We thus focus on the properties observed by STEREO B and Wind in the following contexts. The separation between these two spacecraft is about 0.07 AU. Those discontinuities, which can be identified in both spacecraft measurements, are referred to the major discontinuities of the MC. We will characterize the natures of these major discontinuities in the following subsections, starting from the STEREO B observations due to the clearest MC signatures. In

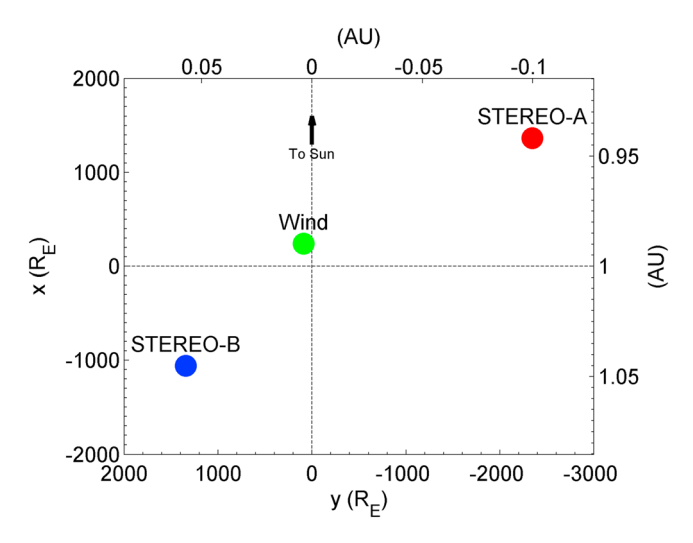


Figure 1. Averaged position of STEREO B (blue), Wind (green), and STEREO A (red) spacecraft on 2007 May 22 in GSE coordinate.

comparison with the measurements between multiple spacecraft, all the quantities derived from STEREO B have been transferred to the GSE coordinate in this study.

2.1. In Situ Observations of STEREO B Spacecraft

Figure 2a presents the STEREO B in situ observations of the MC event during 21–23 May 2007, where the magnetic field and plasma data with 1-min resolution are derived from the IMPACT (Luhmann et al., 2008) and PLASTIC (Galvin et al., 2008) instruments, respectively. From top to bottom show the magnetic field components in GSE coordinate (B_{xr} , B_{yr} , and B_{z}), the magnetic field strength ($|\mathbf{B}|$), the corresponding magnetic field azimuth (ϕ) and latitude (θ) angles, the proton bulk speed (V_p), the total pressure of thermal and magnetic pressures (P_t), the proton number density (N_p), the proton temperature (T_p), and the plasma beta (β). One can see that the magnetic field started rotating at ~04:20 UT on 22 May and was likely to finish at ~04:00 UT on 23 May, although the magnetic field rotation seemed to be interrupted by a high pressure/density structure embedded in the period of 17:30–22:00 UT on 22 May. The signature of field rotation along with the depressed plasma beta satisfies the MC characteristics. By combining with the feature of counterstreaming suprathermal electrons

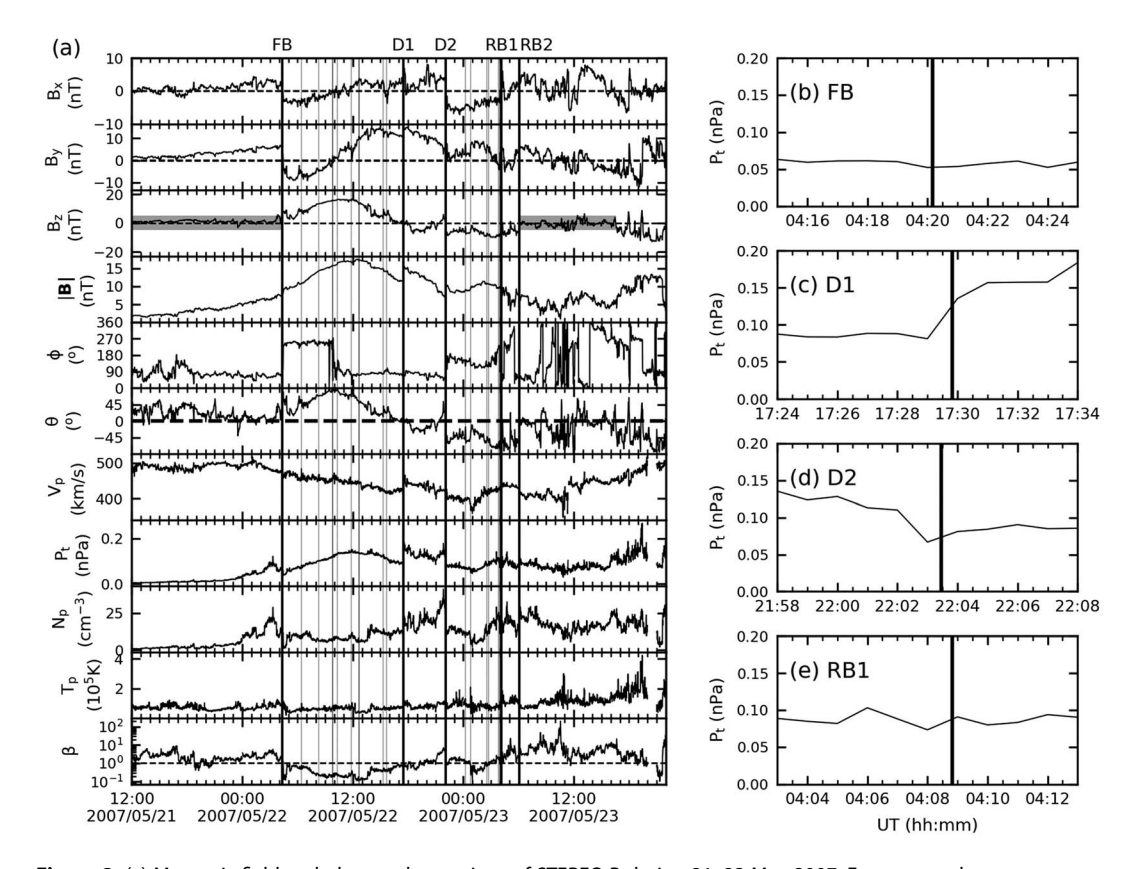


Figure 2. (a) Magnetic field and plasma observations of STEREO B during 21–23 May 2007. From top to bottom are magnetic field components in GSE coordinate (B_{X} , B_{Y} , and B_{Z}), magnetic field strength ($|\mathbf{B}|$), magnetic field azimuth angle (φ) in GSE coordinate, proton bulk speed (V_{p}), total pressure (P_{t}), proton number density (N_{p}), proton temperature (T_{p}), and plasma beta (β). The magnetic field and plasma data are derived from the IMPACT and PLASTIC instruments with 1-min resolution. The gray area indicates the Bz variation of ±5 nT. The black vertical lines denote the times when STEREO B encountered the major discontinuities (FB, D1, D2, RB1, and RB2). The gray vertical lines indicate the time of other internal TDs, which are discussed in section 3. (b–e) Total pressure observation of each major discontinuities except for RB2. The vertical lines indicate the transition time of the discontinuities.



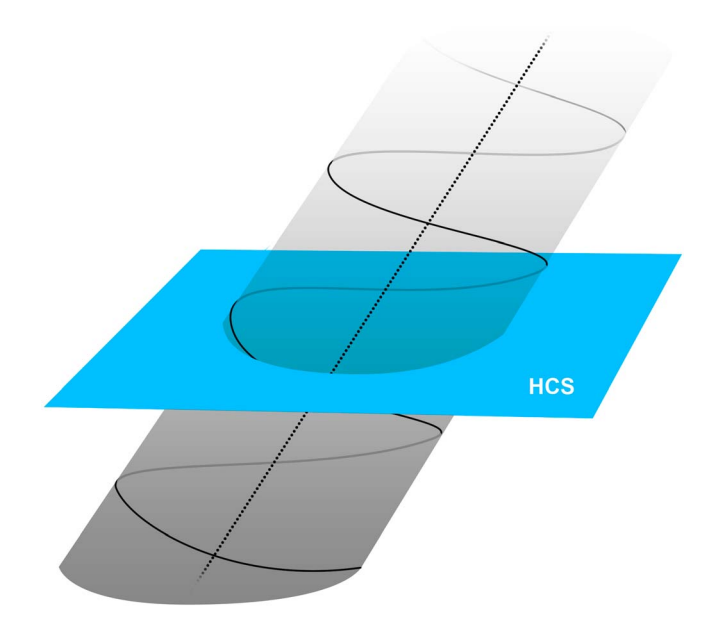


Figure 3. Sketch of the highly-inclined MC embedded in the HCS lying on the ecliptic plane. The helical line denotes the MC magnetic field.

within an MC (see Figure 7 in Chollet et al., 2010), we identify the MC front boundary observed by STEREO B to be at 04:20 UT on 22 May and the rear boundary to be 04:09 UT on 23 May, as labeled by FB and RB1 with vertical lines in Figure 2a, respectively. Both FB and RB1 are TDs with a constant total pressure across the boundary, as shown in Figures 2b and 2e.

Note also that the B_z component outside the MC is very small, as denoted by the gray area in Figure 2a, which implies that the background solar wind is a heliospheric current sheet (HCS) lying on the ecliptic plane. According to the description of force-free flux rope, the magnetic field magnitude theoretically reaches to the maximum at the MC central position. By examining the magnetic field latitude angle (θ) in STEREO B observations, we find that the magnetic field vector has an inclination of ~60° when STEREO B located around the maximum |B| region, suggesting that the studied MC is highly inclined to the ecliptic plane. It should be mentioned that other methods can provide different results of inclination angle with different identification of rear boundary. For example, Möstl, Farrugia, Miklenic, et al. (2009) showed that the inclination angle is in the range of 44°-63° derived by different models. Due to the high inclination of MC axis to the ecliptic plane, the B_{τ} profile can be explained as the MC passing through a HCS seen by STEREO B, which is sketched in Figure 3. It was shown that the high-inclination MC possibly has an elongated cross section (e.g., Crooker & Intriligator, 1996). We also identify another boundary RB2 at 06:00 UT on 23 May to be the rear boundary of

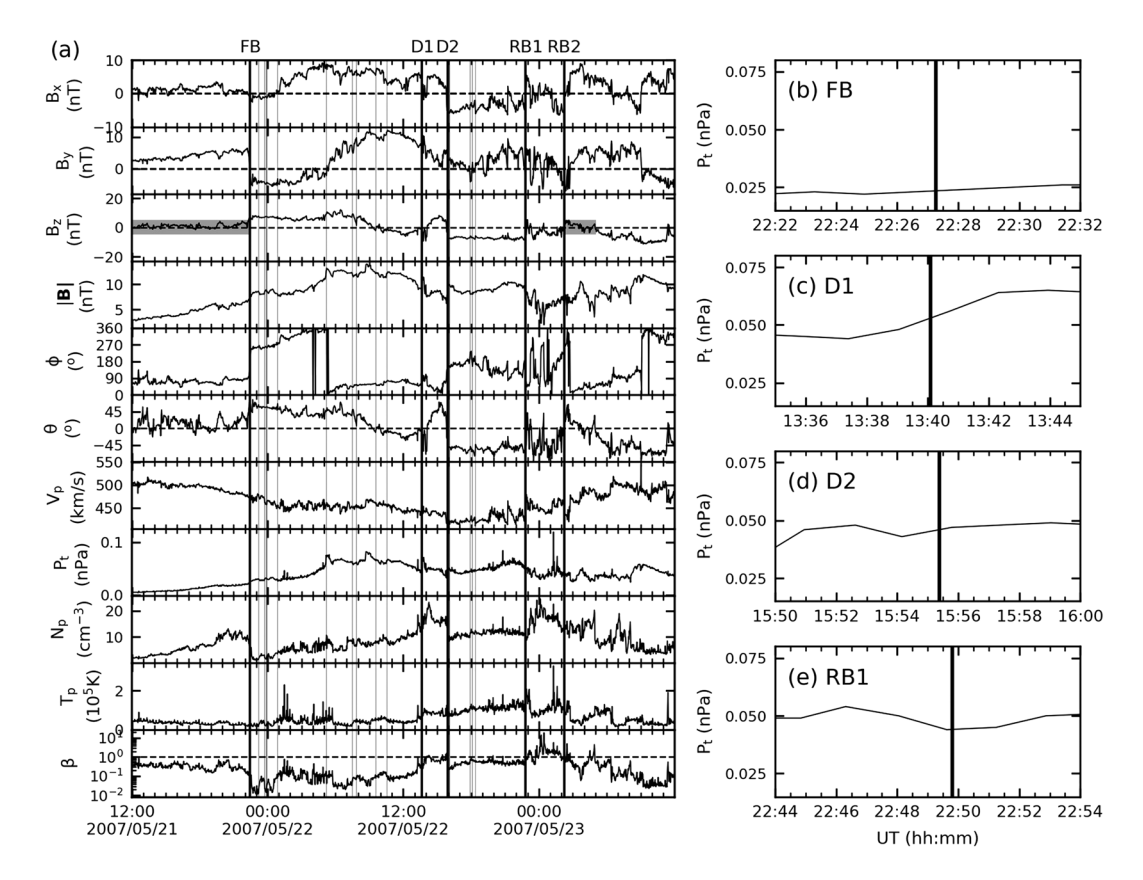


Figure 4. (a) Magnetic field and plasma observations of Wind spacecraft during 21–23 May 2007 with the same format as Figure 2. The magnetic field and plasma data are derived from the MFI and SWE instrument with 92-s resolution. (b–e) Total pressure observations of each major discontinuities measured by Wind except for RB2. The format is that same as Figure 2.

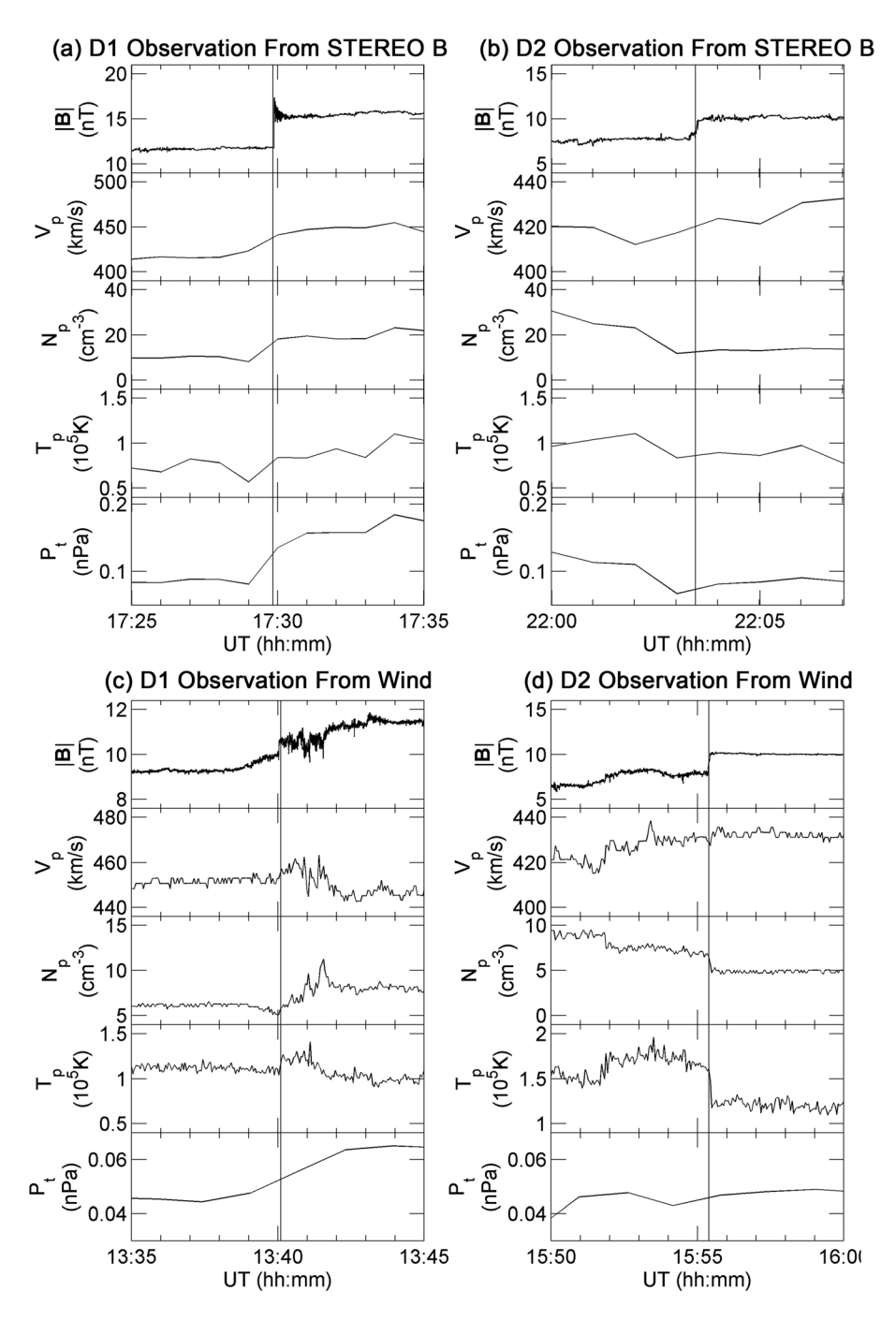


Figure 5. (a-b) STEREO B observations across the D1 and D2 on 22 May 2007, where the magnetic field data have 8-Hz resolution. (c-d) Wind observations around the D1 and D2 on 22 May 2007 with the 11-Hz magnetic field data. The vertical line denotes the transit time of the shock/discontinuity structure.

the whole structure embedded in the HCS based on the feature of long-lasting small B_z . The interval between RB1 and RB2 is the transition region from the MC main body to the background HCS. In addition, two other obvious shock/discontinuity structures inside the MC are found, which are the D1 at 17:29 UT on 22 May and D2 at 22:03 on 22 May. Apparently, D1 and D2 are the boundaries enclosed the high pressure/density region. The total pressure across the D1 and D2 are shown in Figures 2c and 2d and will be analyzed in detail in the section 2.3.

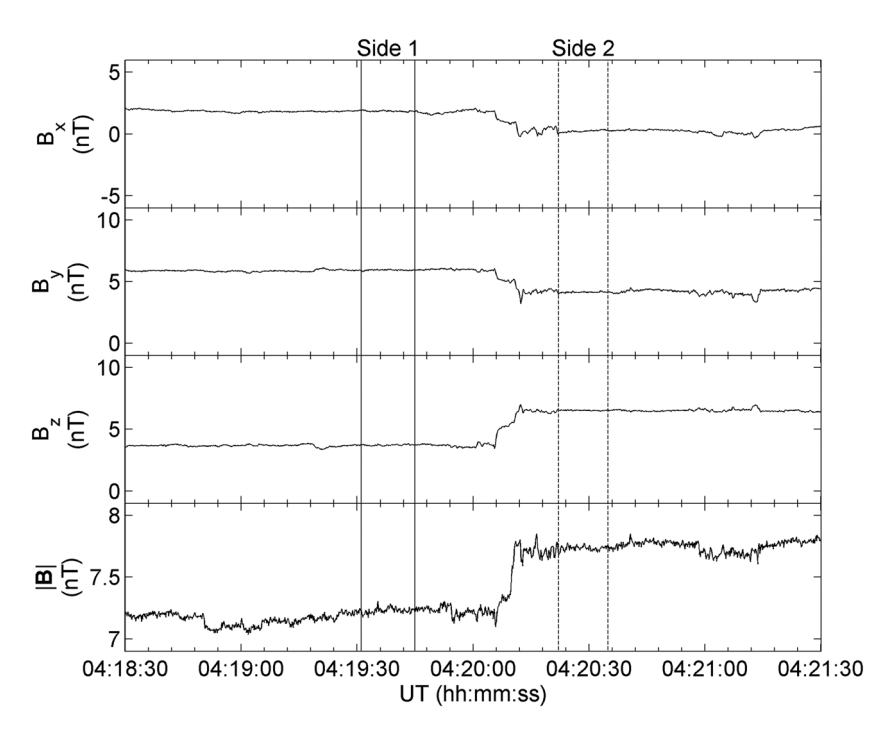


Figure 6. High-resolution (8 Hz) magnetic field observations of STEREO B around the FB on 22 May 2007. The solid (dashed) lines enclose the time interval of side 1 (side 2) for TD normal calculation.

2.2. In Situ Observations of Wind Spacecraft

Figure 4a presents the Wind observations of the MC event during 21–23 May 2007, where the magnetic field and plasma data with 92-s resolution are derived from the MFI (Lepping et al., 1995) and SWE (Ogilvie et al., 1995) instruments, respectively. One can see that the magnetic field started rotating at 22:14 UT on 21 May along with the decrease of plasma beta, which is identified as the FB. The field rotation seemed to end at 22:49 UT on 22 May (i.e., RB1), although a high-density region was found during 13:39–15:55 UT on 22 May. Both FB and RB1 are TDs according to the feature of constant total pressure across the boundary shown in Figures 4b and 4e. Moreover, with the help of the background HCS structure denoted by the gray area of B_z in Figure 4a, we suggest that Wind spacecraft encountered the RB2 at 02:14 UT on 23 May. The large magnetic field fluctuations appeared between RB1 and RB2 is an indicator of the transition region from MC to HCS. Based on the large-scale relationship between MC and background solar wind shown in the temporal variation of magnetic fields, we thus conclude that both STEREO B and Wind spacecraft observed the same event when the MC propagated in the interplanetary space.

Besides FB, RB1, and RB2, the high-density region is enclosed by two discontinuities, that is, D1 at 13:39 UT on 22 May and D2 at 15:55 UT on 22 May. The total pressure profiles across the D1 and D2 observed at Wind are shown in Figures 4c and 4d. Note that there is no apparent pressure change across the D2. Moreover, no corresponding high-pressure region is found at Wind position. Such different features in Wind and STEREO B observations can be due to the inhomogeneity of pressure pulse possibly produced by local magnetic field structures. The increased density appeared at both spacecraft may indicate that they come from the same source. Therefore, when two spacecraft passed through different parts of the pressure pulse region, they can measure different pressure profiles. This MC event has also been reported in some event lists (http:// www-ssc.igpp.ucla.edu/~jlan/ACE/Level3/ICME_List_from_Lan_Jian.pdf, https://wind.nasa.gov/2007.php, and http://space.ustc.edu.cn/dreams/wind_icmes/). However, most of the previous studies use D1 as the rear boundary (e.g., Kilpua et al., 2009, and reference therein), which is different from this study. The details of the comparison between different identifications of MC rear boundary will be discussed later. These five structures (FB, D1, D2, RB1, and RB2) are referred to the major discontinuities in this study. But since RB2 is the boundary between transition region and HCS and is not directly related to the MC main body, we focus on the properties of four remaining structures in the following section.



Table 1Normal Directions of Shocks/Discontinuities Observed by STEREO B and Wind in GSE Coordinate

	Obs. time		$\widehat{\mathbf{n}}_{TD}$,	ε _{TD} (°)	$\widehat{\mathbf{n}}_{SH}, \epsilon_{SH}$ (°)		
	STEREO B	Wind	STEREO B	Wind	STEREO B	Wind	
FB D1 D2 RB1	22 May 2007 04:20 22 May 2007 17:29 22 May 2007 22:03 23 May 2007 04:09	21 May 2007 22:14 22 May 2007 13:39 22 May 2007 15:55 22 May 2007 22:49	(0.88, 0.42, 0.23), 2.0 (0.17, -0.05, 0.98), 4.3 (0.69, -0.29, -0.67), 15.5 (0.91, -0.40, 0.04), 10.6	(0.10, -0.03, 0.08), 3.7 (0.14, -0.05, -0.986), 35.0 (0.83, 0.18, -0.53), 31.6 (0.79, -0.53, -0.30), 8.7	- (0.97, -0.14, 0.19), 20.5 (0.22, 0.96, -0.18), 11.1 -	- (0.85, 0.32, 0.42), 44.1 (0.41, -0.83, 0.37), 6.1 -	

2.3. Shock/Discontinuity Analysis of D1 and D2

Figures 5a and 5b display the STEREO B observations across the D1 and D2, where the IMPACT magnetic field data have a high-resolution of 8 Hz and the PLASTIC plasma data have 1-min resolution. Similarly, Figures 5c and 5d present the high resolution plots of D1 and D2 measurements by Wind, where the MFI magnetic field data have 11-Hz resolution and the 3DP plasma data have 3-s resolution. For D1, STEREO B observed a clear increase in magnetic field strength, proton bulk speed, proton number density, and proton temperature at ~17:30 UT. All quantities then approached to a steady state. It is suggested that D1 is a forward fast shock based on the Rankine-Hugoniot (R-H) relations. Wind spacecraft also observed a clear increase in magnetic field strength and plasma quantities at ~13:40 UT but with more turbulent fields at both sides of D1. All parameters then change to a different state at ~13:42 UT. We thus suppose that the D1 structures seen at Wind and STEREO are different types of fast shock, which will be discussed in detail in the later section.

For D2, both spacecraft observed similar profiles that the magnetic field strength enhanced sharply, the proton bulk speed increased slightly, and the proton number density and temperature decreased. However, the total pressure did not have the clear change pattern across the D2. Since the contributions of electron and helium components and the anisotropy of the thermal pressure in solar wind are not taken into account in the total pressure calculation, we cannot determine the D2 as a slow shock accurately. It is thus suggested that D2 is possibly either a reverse slow shock or a TD (Feng, Lin, et al., 2008; Lin et al., 2009).

To solve the ambiguity of D2 structure and to confirm that all the shocks or discontinuities are identified correctly, we further determine the normal direction of each shock/discontinuity and also estimate its propagation time from Wind to STEREO B. By assuming that the shock/discontinuity is an infinite plane surface moving with the speed V in the normal direction $\hat{\bf n}$, the propagation time can be calculated by

$$\tau = \Delta \mathbf{R} \cdot \frac{\widehat{\mathbf{n}}}{V},\tag{1}$$

where $\Delta \mathbf{R}$ is the displacement vector between the two spacecraft.

Knetter et al. (2004) found from Cluster observations that almost all the analyzed discontinuities except shocks have very small normal component of magnetic field regardless of the discontinuity type. It implies that the TD normal direction $\hat{\mathbf{n}}_{TD}$ determined by the cross product of the magnetic fields on both sides,

namely, $\hat{\textbf{n}}_{TD} = \pm \frac{(\textbf{B}_1 \times \textbf{B}_2)}{|\textbf{B}_1 \times \textbf{B}_2|}$, can represent the normal of all types of discontinuities except shocks. The \textbf{B}_1

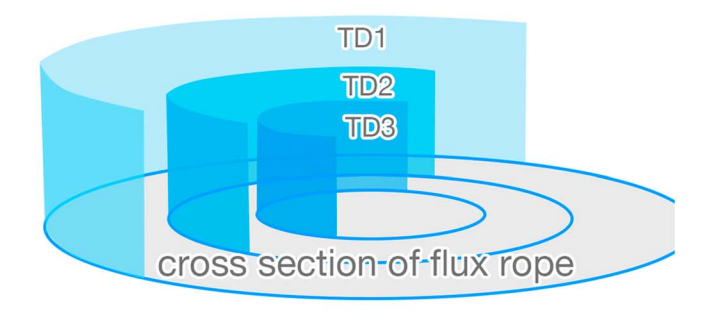
and ${\bf B}_2$ are the averaged magnetic fields on sides 1 and 2, respectively, which are determined from the high-resolution data by selecting the time interval with relatively steady magnetic field variations without obviously large fluctuations. As illustrated in Figure 6, the vertical solid lines enclose the selected time interval

Table 2Comparison of Observed and Estimated Propagation Time

compani	Companion of Coscived and Estimated Propagation Time							
	t_{TD}	τ_{o} (min)	τ _{TD} (min)	Δau_{TD} (%)	t _{SH}	τ _{SH} (min)	Δau_{SH} (%)	
FB	22 May 2007 03:10	366	296	19.1	-	-		
D1	22 May 2007 22:27	230	528	129.6	22 May 2007 17:06	207	10.1	
D2	22 May 2007 19:47	368	232	37.0	23 May 2007 07:39	944	156.8	
RB1	23 May 2007 07:02	320	493	54.1	-	_		







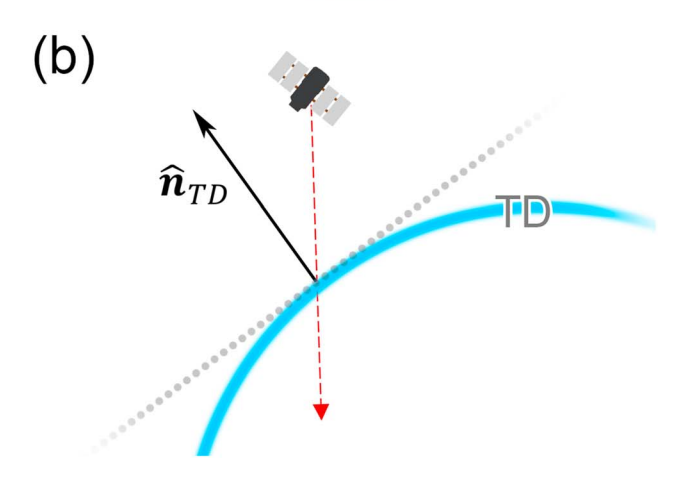


Figure 7. (a) Illustration of TD planes (TD1-3) wrapping around the center axis of flux rope. (b) Sketch of the spatial relationship between the internal TD plane, TD normal, and spacecraft trajectory. The blue curve represents a segment of the TD cross section on the ecliptic plane and the red dashed line denotes the spacecraft trajectory. The dashed gray line indicates the line tangent to the TD plane at the spacecraft position, which is perpendicular to the TD normal direction $\hat{\pmb{n}}_{TD}$ (black arrow).

of side 1 and the dashed lines enclose the interval of side 2. The TD propagating speed, $V_{\rm TD}$, is then calculated from the component of solar wind velocity in the TD normal direction

$$V_{TD} = \mathbf{V}_{1 \text{ or } 2} \cdot \hat{\mathbf{n}}_{TD}, \tag{2}$$

where $\mathbf{V}_{1\text{ or }2}$ are the averaged solar wind velocity on side 1 or side 2. For a shock structure, the normal direction $\widehat{\mathbf{n}}_{\text{SH}}$ is obtained from the coplanarity theorem by $\widehat{\mathbf{n}}_{\text{SH}} = \pm (\mathbf{B}_u \times \mathbf{B}_d) \times (\mathbf{B}_u - \mathbf{B}_d) / |(\mathbf{B}_u \times \mathbf{B}_d) \times (\mathbf{B}_u - \mathbf{B}_d)|$ (Colburn & Sonett, 1966), where \mathbf{B}_u and \mathbf{B}_d represent the upstream and downstream magnetic fields, respectively. And the shock speed is derived from the mass continuity equation

$$V_{SH} = \mathbf{V}_{SH} \cdot \widehat{\mathbf{n}}_{SH} = \frac{(n_{d}\mathbf{V}_{d} - n_{u}\mathbf{V}_{u}) \cdot \widehat{\mathbf{n}}_{SH}}{n_{d} - n_{u}},$$
(3)

where the $n_{\rm d}$ ($n_{\rm u}$) and ${\bf V}_{\rm d}$ (${\bf V}_{\rm u}$) are the number density and solar wind velocity at the shock downstream (upstream) region.

Table 1 summarizes the normal directions of four identified structures in GSE coordinate obtained from STEREO B and Wind measurements by taking FB and RB1 as TDs and by assuming D1 and D2 as TDs or shocks. The estimation uncertainties of the corresponding normal directions are presented in terms of the error cone angles ϵ_{TD} and ϵ_{SH} . In short, the error cone includes the possible variations of normal directions caused by magnetic field fluctuations within a certain time interval around a TD or a shock. The derived normal direction ($\hat{\mathbf{n}}_{TD}$ or $\hat{\mathbf{n}}_{SH}$) is the central axis of the corn with the uncertainty (ϵ_{TD} and ϵ_{SH}) as the size of the cone angle. Different methods are applied for ε_{TD} and ε_{SH} estimations due to the different properties of TDs and shocks. We thus do not compare the error cone sizes between TDs and shocks. It can be seen in Table 1 that the estimated ε_{TD} are relatively small except for D1 and D2 derived by Wind observations. Moreover, we obtain the larger values of ε_{SH} . We suggest that the error estimation for TDs provided here is smaller than that using the convention method (e.g., minimum variance analysis and cross product). The detailed derivations of ε_{SH} and ε_{TD} are given in Appendices A and B.

We further calculate the arrival times (t_{TD} and t_{SH}) of these four structures at the STEREO B. Their propagation times, τ_{TD} and τ_{SH} , from Wind to STEREO B and the corresponding errors compared with the measured propagation time (τ_o) are also given in Table 2. The estimated error of propagation time is defined by $\Delta \tau_{TD} = |\tau_{TD} - \tau_o|/\tau_o$ or $\Delta \tau_{SH} = |\tau_{SH} - \tau_o|/\tau_o$. We found that the estimated error is much larger if the D2 is taken as a reverse slow shock or the D1 is taken as a TD. We thus conclude that D2 is a TD rather than a reverse slow shock. In other words, it is difficult to distinguish a structure is a TD or a slow shock only based on single-spacecraft observations as pointed out by Feng, Lin, et al. (2008). We propose that such ambiguity can be resolved by multispacecraft measurements.

3. Internal TDs for MC Configuration Construction

Since the helical field topology of an MC can be described by a force-free flux-rope model with the feature of no radial magnetic field component, an MC can be regarded as the structureas the structure of multiple of multiple cylindrical TDs wrapping around the central axis of the cloud, as sketched by the cylindrical blue planes in Figure 7a. When a spacecraft passes through such an internal TD, the orientation of TD normal derived from the spacecraft measurement should be perpendicular to the local tangent surface at the spacecraft location, as denoted by the dashed gray line in Figure 7b. In other words, the normal estimations of internal TDs enable us to deduce the possible topologies of MC along the spacecraft trajectory.

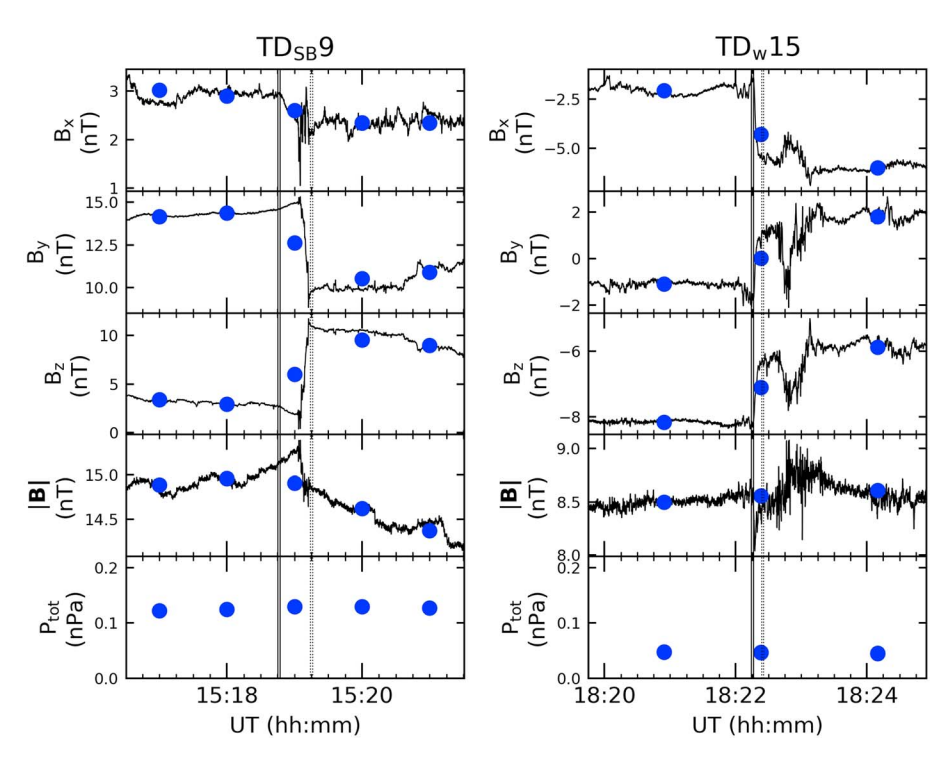


Figure 8. Magnetic field observations of (a) $TD_{SB}9$ on 22 May with a resolution of 8 Hz and (b) $TD_{W}15$ on 22 May with a resolution of 11 Hz. The solid and dashed lines enclose the time intervals of sides 1 and 2 for the TD normal calculations, respectively. The blue dots indicate the magnetic field and plasma data with 1-min resolution.

According to our scenario, a spacecraft is supposed to detect numerous TDs during the passage of the MC. Among these successively TDs, we arbitrarily select some cases based on the high-resolution magnetic field measurements of STEREO B and Wind. In general, the temporal variation of low-resolution data (e.g., 1 min) should have consistent tendency with the high-resolution one. But the high-resolution data should provide a more reliable determination of the TD normal direction. Figure 8 illustrates two examples, TD_{SB} 9 and TD_{W} 15, showing different situations when using high-resolution (black curve) and 1-min resolution (blue dot) magnetic field data for TD normal estimation, where the subscripts SB and W represent the TD observed by STEREO B and Wind, respectively. Note that unlike the major discontinuities, all the internal TDs are identified

Table 3Selected TDs Inside the MC Observed by STEREO B

ID	Obs. time	$\widehat{\mathbf{n}}_{TD}$	ε _{TD} (°)	θ ₁₂ (°)	
TD _{SB} 1	22 May 2007 06:25:48	(0.53, 0.63, 0.57)	10	10.2	
$TD_{SB}2$	22 May 2007 08:16:43	(0.74, 0.59, 0.32)	2.6	4.3	
TD _{SB} 3	22 May 2007 09:47:52	(0.97, -0.26, 0.01)	3.0	14.2	
TD _{SB} 4	22 May 2007 09:49:37	(0.99, -0.04, -0.02)	2.6	15.6	
TD _{SB} 5	22 May 2007 10:19:39	(0.12, 0.99, -0.05)	3.0	8.0	
$TD_{SB}6$	22 May 2007 11:49:05	(0.95, -0.30, 0.02)	3.4	7.3	
$TD_{SB}7$	22 May 2007 12:39:05	(0.83, -0.52, 0.21)	2.0	5.2	
TD _{SB} 8	22 May 2007 12:41:12	(0.77, 0.38, -0.51)	2.9	3.6	
TD _{SB} 9	22 May 2007 15:19:08	(0.98, -0.20, -0.02)	1.6	37.4	
TD _{SB} 10	22 May 2007 15:41:54	(0.72, 0.36, -0.60)	9.2	2.6	
TD _{SB} 11	23 May 2007 00:15:25	(0.85, 0.35, -0.39)	4.4	53.8	
TD _{SB} 12	23 May 2007 00:47:16	(0.77, 0.12, -0.62)	5.6	32.7	
TD _{SB} 13	23 May 2007 02:32:51	(0.82, 0.58, 0.05)	11.2	7.8	
TD _{SB} 14	23 May 2007 02:43:25	(0.79, -0.37, -0.50)	5.3	13.4	
TD _{SB} 15	23 May 2007 03:48:54	(0.92, -0.34, -0.22)	4.1	15.4	
TD _{SB} 16	23 May 2007 03:57:37	(0.91, -0.35, -0.23)	8.7	22.8	
TD _{SB} 17	23 May 2007 03:58:25	(0.91, -0.35, -0.23)	8.5	53.8	

independently at two spacecraft. The vertical solid and dashed lines indicate the side 1 and side 2 regions of the TD in high-resolution data. It can be seen that the magnetic fields at both sides of $TD_{SB}9$ are relatively stable. We thus obtain very similar TD normal using either the 8-Hz or 1-min resolution data. However, TD_W15 is followed by a fine structure at ~18:23 UT giving a large difference of magnetic field profiles between the 11-Hz and 1-min data. This fine structure will be included in the normal estimation of TD_W15 when using 1-min data, which results in the unreliable TD normal direction. Therefore, we use the high-resolution magnetic field data to determine the normal orientations of internal TDs in this study.

The internal TDs identified from STEREO B and Wind are listed in Tables 3 and 4 and also denoted as the gray vertical lines in Figures 2a and 4a. The ϵ_{TD} in Tables 3 and 4 represents the error cone angle of the corresponding TD and the θ_{12} indicates the angle between magnetic fields at two sides of TD (i.e., \boldsymbol{B}_1 and \boldsymbol{B}_2). A tendency is found that the estimation uncertainty ϵ_{TD} is small for large θ_{12} , and the ϵ_{TD} is getting larger when the θ_{12} becomes smaller, as expected from the cross-product calculation result.



Table 4
Selected TDs Inside the MC Observed by Wind

Selected 1Ds Inside the MC Observed by Wind						
ID	Obs. time	$\widehat{\mathbf{n}}_{TD}$	ε _{TD} (°)	θ ₁₂ (°)		
TD _w 1	21 May 2007 23:12:56	(0.91, 0.32, 0.26)	2.1	14.7		
TD_w2	21 May 2007 23:44:37	(0.82, -0.53, -0.20)	2.2	3.3		
TD_w3	21 May 2007 23:55:15	(0.82, 0.43, 0.38)	1.8	4.7		
TD_w4	21 May 2007 23:56:10	(0.96, 0.12, 0.26)	3.8	2.5		
TD_w5	22 May 2007 00:54:23	(0.79, 0.56, 0.26)	7.4	12.9		
$TD_{w}6$	22 May 2007 05:13:37	(0.74, 0.14, -0.66)	8.7	10.9		
TD_w7	22 May 2007 07:31:22	(0.52, -0.84, 0.16)	2.9	1.8		
TD_w8	22 May 2007 07:52:59	(0.82, -0.57, -0.06)	4.8	36.8		
TD_w9	22 May 2007 09:34:18	(0.74, -0.47, -0.48)	2.4	12.3		
TD_w10	22 May 2007 10:35:30	(0.84, -0.14, 0.52)	1.5	2.8		
TD _w 11	22 May 2007 16:05:23	(0.62, -0.47, -0.63)	3.1	10.3		
TD_w12	22 May 2007 16:06:16	(0.41, -0.70, -0.59)	3.3	13.5		
TD_w13	22 May 2007 17:54:17	(0.84, 0.12, -0.53)	6.0	6.0		
TD _w 14	22 May 2007 18:07:03	(0.88-0.13-0.46)	6.4	22.2		
TD _w 15	22 May 2007 18:22:17	(0.45, 0.86, -0.24)	4.4	35.3		

Figure 9 shows the temporal variations of normal directions of internal TDs projected on the ecliptic plane. The top panel shows the normal variation of TD_{SB}1–17 and the bottom panel is for TD_W1–15. The gray area indicates the time interval when the spacecraft transited the high pressure/density region. Since these internal TDs are supposed to be warping around the MC central axis, the normal directions of successive TDs should vary gradually without changing abruptly between adjacent TDs. However, we notice that in Figure 9, for instance, the orientation of TD_{SB}5 is guite different from that of TD_{SB}4 and TD_{SB}6. We suggest that this abnormal direction of TD orientation is probably associated with the surface wave or disturbance on the TD plane (Hollweg, 1982). As illustrated in Figure 10, even though three adjacent disturbed TD planes are parallel, the measured normal of TD_{SR}5 can be different from the others when the spacecraft passes through the different parts of local disturbed region. Therefore, instead of using individual TD normal, we suggest using the most representative TD within a certain time interval to deduce the MC topology when spacecraft passage a certain section of the MC.

4. Results

4.1. Determination of a Common TD Normal

Based on the idea that the adjacent TDs inside an MC have similar orientations and there is no normal magnetic field (B_n) across a TD, the strength of magnetic fields along the normal direction of an internal TD should approach to zero. Moreover, such feature should last for a certain period of time around the TD. In this study, we examine the time variation of $B_n/|\mathbf{B}|$ by imposing the normal direction of a specific TD to the whole MC period. Once the evaluated $B_n/|\mathbf{B}|$ remains close to zero for a sufficiently long time interval, this TD is determined as the common TD for this period when spacecraft passage a certain section of the MC. It is expected that several sections with different but gradual changes of TD orientations are detected during the MC transit. By combining all the identified common TDs, we can infer the MC magnetic field topology along the spacecraft trajectory from the TD orientations varying from one section to another section.

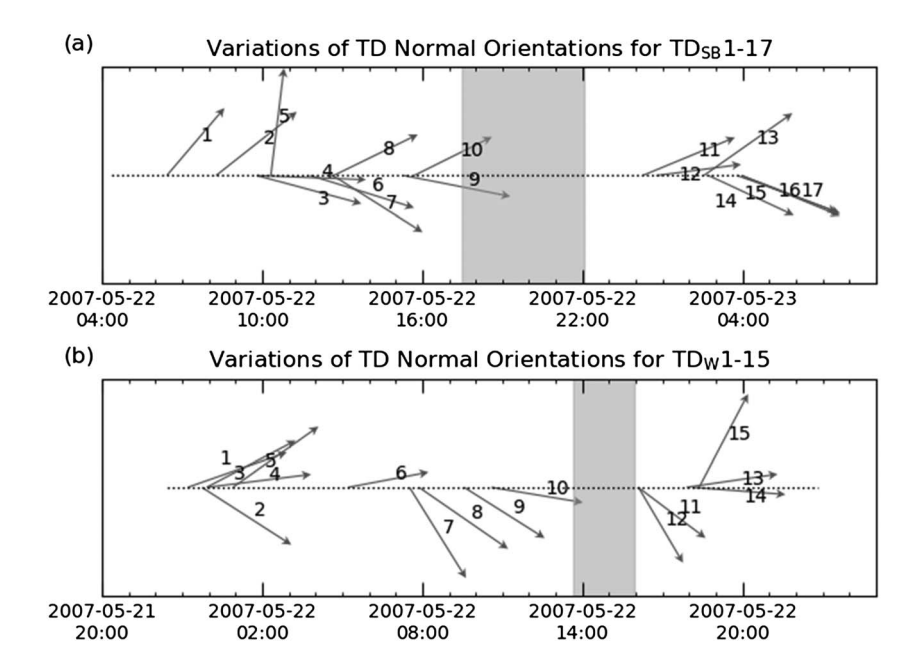


Figure 9. Normal orientations of identified (a) $TD_{SB}1-17$ and (b) $TD_{W}1-15$ projected on the ecliptic plane, where the number labels the TD ID in Tables 3 and 4. The gray area denotes the time interval when spacecraft passed through the high pressure/density region and the horizontal dotted line indicate the spacecraft trajectory.

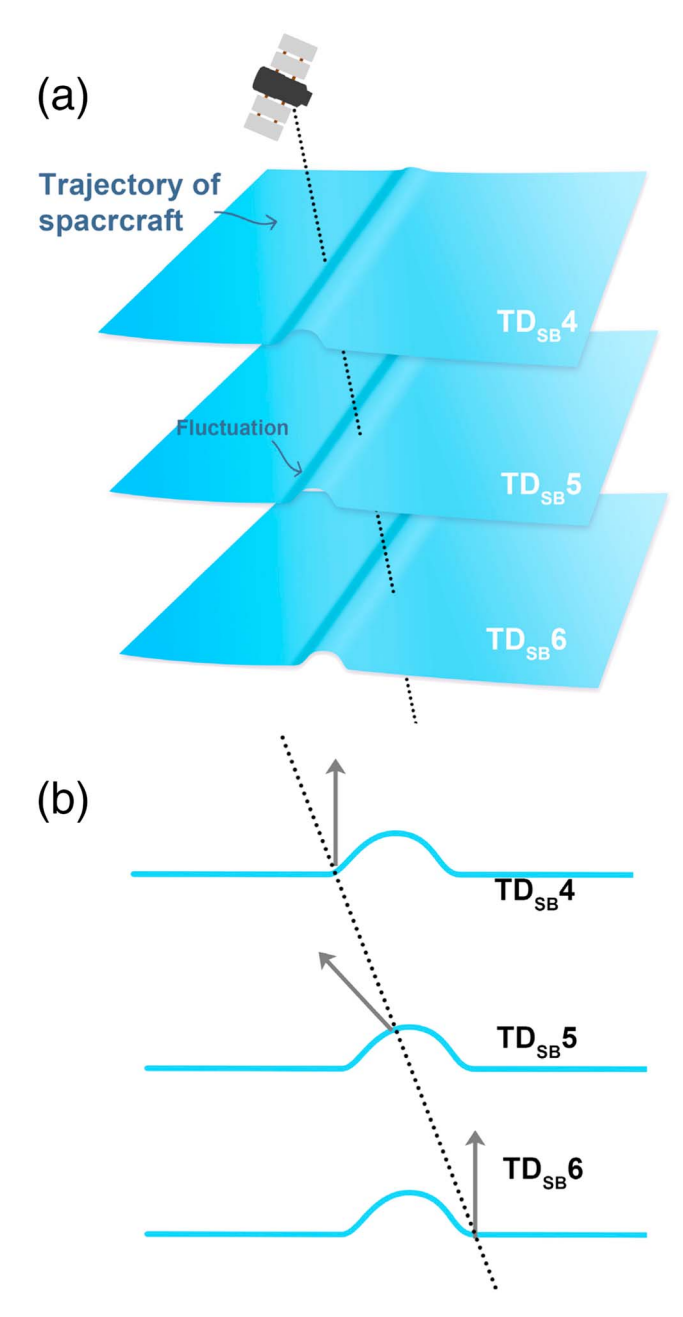


Figure 10. (a) Illustration of abnormal TD normal direction due to local fluctuation on the TD plane. (b) Side view of (a). The arrow indicates the normal direction measured along the spacecraft trajectory (dotted line).

Figures 11a and 11b show the variations of $B_n/|\mathbf{B}|$ estimated from different normal directions of the common TDs measured by STEREO B and Wind, respectively. The gray area indicates the time interval of the high pressure/density region. We find that TD_{SB}3 is the common TD before STEREO B encountered the high pressure/density region, as shown in the top panel of Figure 11a. The $B_n/|\mathbf{B}| \cong 0$ (yellow area) lasts few hours with an average of -0.07 and fluctuation size of ± 0.08 till the front boundary of high pressure/density region (i.e., D1) is observed, where B_n now is the magnetic field component in the direction of TD_{SB}3 normal. It means that the normal orientation of the TDs inside this region deviates from TD_{SB}3 with an averaged angle of -4° and with a $\pm 5^{\circ}$ fluctuation angle, implying that the TDs in this time period have very similar orientations. After STEREO B passed through the high pressure/density region, our result shows that TD_{SB}11 becomes the common TD of this section, as presented in the bottom panel of Figure 11a. The averaged $B_p/|\mathbf{B}|$ in this section is 0.04 with the fluctuation size of ±0.18, which means that the common TD normal deviates from the TD_{SB}11 normal with an averaged angle of 2° and with a ±11° in fluctuation angle. After examining the averaged deviation and fluctuation angle from all the identified TDs, we confirm that TD_{SB}3 and TD_{SB}11 can represent the orientations of the TDs inside the MC. Consequently, the MC in STEREO B observation can be roughly divided into two sections that the TD orientation before high pressure/density region is close to the TD_{SB}3 direction and then changes to the TD_{SB}11 direction after the passage of the high pressure/density region.

In the same manner, the MC in Wind observation can be divided into four sections. Panels from top to bottom in Figure 11b display the $B_{\text{n}}/$ | \mathbf{B} | variations derived from the normal directions of TD_W3, TD_W6, TD_W8, and TD_W11, respectively. The averaged deviation angles from the normal directions of common TDs in each section are 3°, -1°, 0°, and 1°, respectively. The corresponding fluctuation sizes are ± 8 °, ± 11 °, ± 4 °, and ± 12 °, showing that we identify the appropriate common TDs in each section. The continuous connection of time interval between adjacent sections implies that the orientation of the internal TDs varies gradually from the TD_W3 direction to the TD_W11 direction.

4.2. Magnetic Field Configuration of the MC Along the Spacecraft Trajectories

After determining the common TD and its normal direction in each section from the $B_n/\mid \mathbf{B}\mid \cong 0$ criterion, we further trace the variations of TD orientations along the spacecraft trajectory. Remembering that the internal TD should be tangent to the flux-rope cross section at the spacecraft location, as illustrated in Figure 7b, the intersection between the common TD plane and the ecliptic plane should be a tangent to the MC magnetic field con-

figuration on the ecliptic plane at the spacecraft location. Figure 12a shows the temporal variations of these intersection lines when spacecraft passage different parts of the MC from FB to RB1. One can see that before the high pressure/density region, the TD planes almost have the same orientation in STEREO observations, while the TD planes in Wind observations apparently turn into another direction after ~06:00 UT on 22 May. The TD planes still have different orientations between STEREO B and Wind even after the high pressure/density region. In particular, STEREO B detected quiet different TD orientations before and after the high pressure/density region with the line slope in Figure 12a changing from positive to negative. Such differences may imply that these two spacecraft passed through the different parts of MC and thus observed the different variation patterns of flux-rope structure.

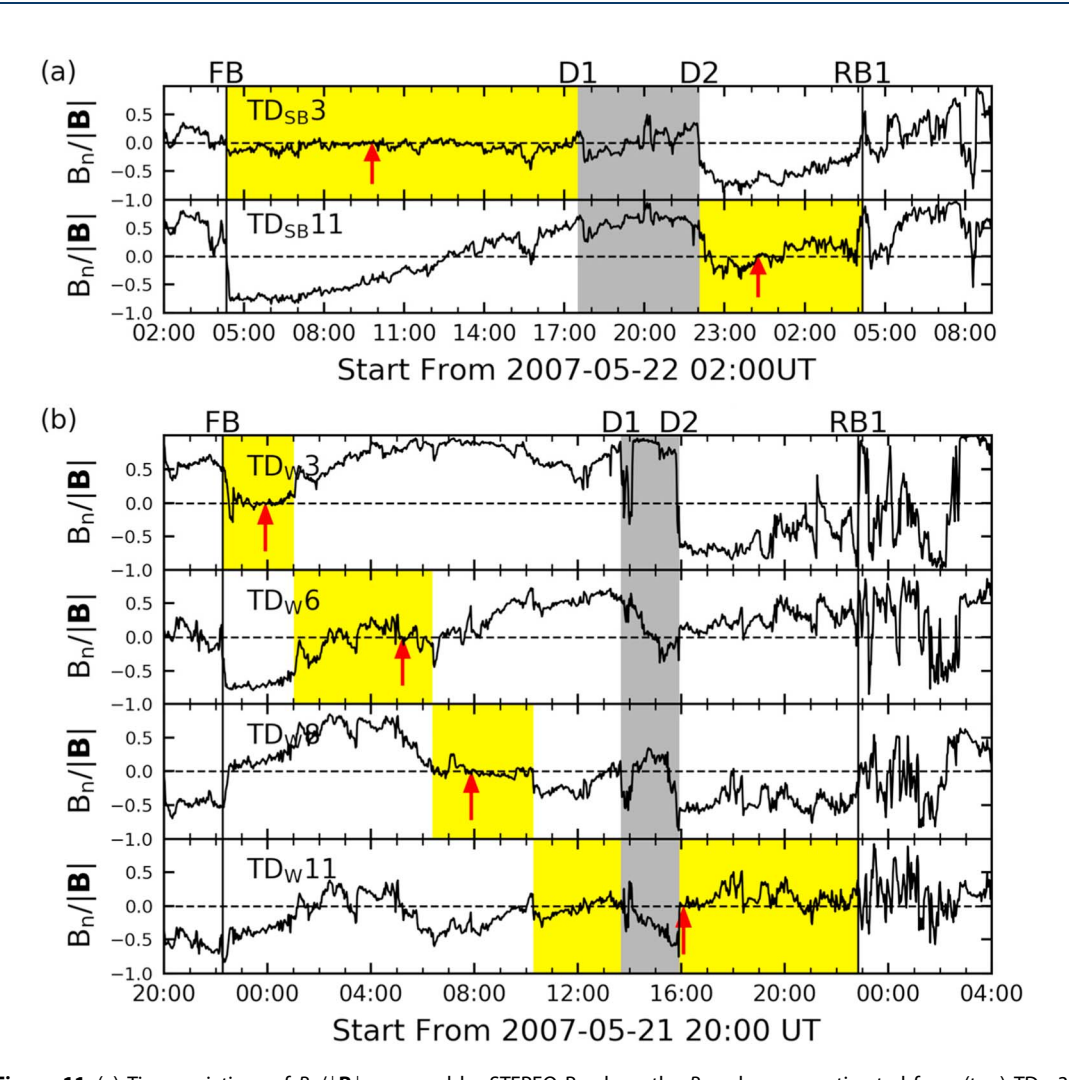


Figure 11. (a) Time variations of $B_n/|\mathbf{B}|$ measured by STEREO B, where the B_n values are estimated from (top) TD_{SB}3 and (bottom) TD_{SB}11. (b) Time variations of $B_n/|\mathbf{B}|$ measured by Wind. The B_n values from top to bottom are calculated from TD_W3, TD_W6, TD_W8, and TD_W11, respectively. The yellow area indicates the time interval of small $B_n/|\mathbf{B}|$, and the gray area denotes the time interval when spacecraft transited the high pressure/density region. The red arrows in each panel indicate the time of the corresponding common TDs.

According to the description provided by Richardson et al. (1998), the interplanetary magnetic fields at 1 AU can be considered as planar structures within a distance of 10 Earth radii. Since the separation between STEREO B and Wind is ~0.07 AU, corresponding to more than 100 Earth radii, it is reasonable to assume that the MC observed both by STEREO B and Wind has the curvature morphology of magnetic fields, although we cannot reconstruct the MC large-scale morphology from our TD derivations. Note that the TD orientations detected at STEREO B show the "hill" variation pattern in Figure 12a, while those detected at Wind have the "valley" variation pattern. By assuming that the cross-section shape of MC has simple geometry without deforming during the propagation, it can be explained that STEREO B and Wind passed through two different sides of MC central axis regardless of the MC cross-section shape (e.g., circular or elliptical), as sketched in Figure 12b. Such interpretation is correct only for the RB1 being as the MC rear boundary. If the MC rear boundary changes to the D1, however, STEREO B is supposed to transit the MC central area according to the same orientation of TDs derived before the high pressure/density region. The Wind spacecraft should transited away from the MC central area based on the valley variation pattern of TD orientations, as sketched in Figure 12c. In other words, the magnetic field morphology on the MC cross section strongly depends on the determination of MC boundaries.



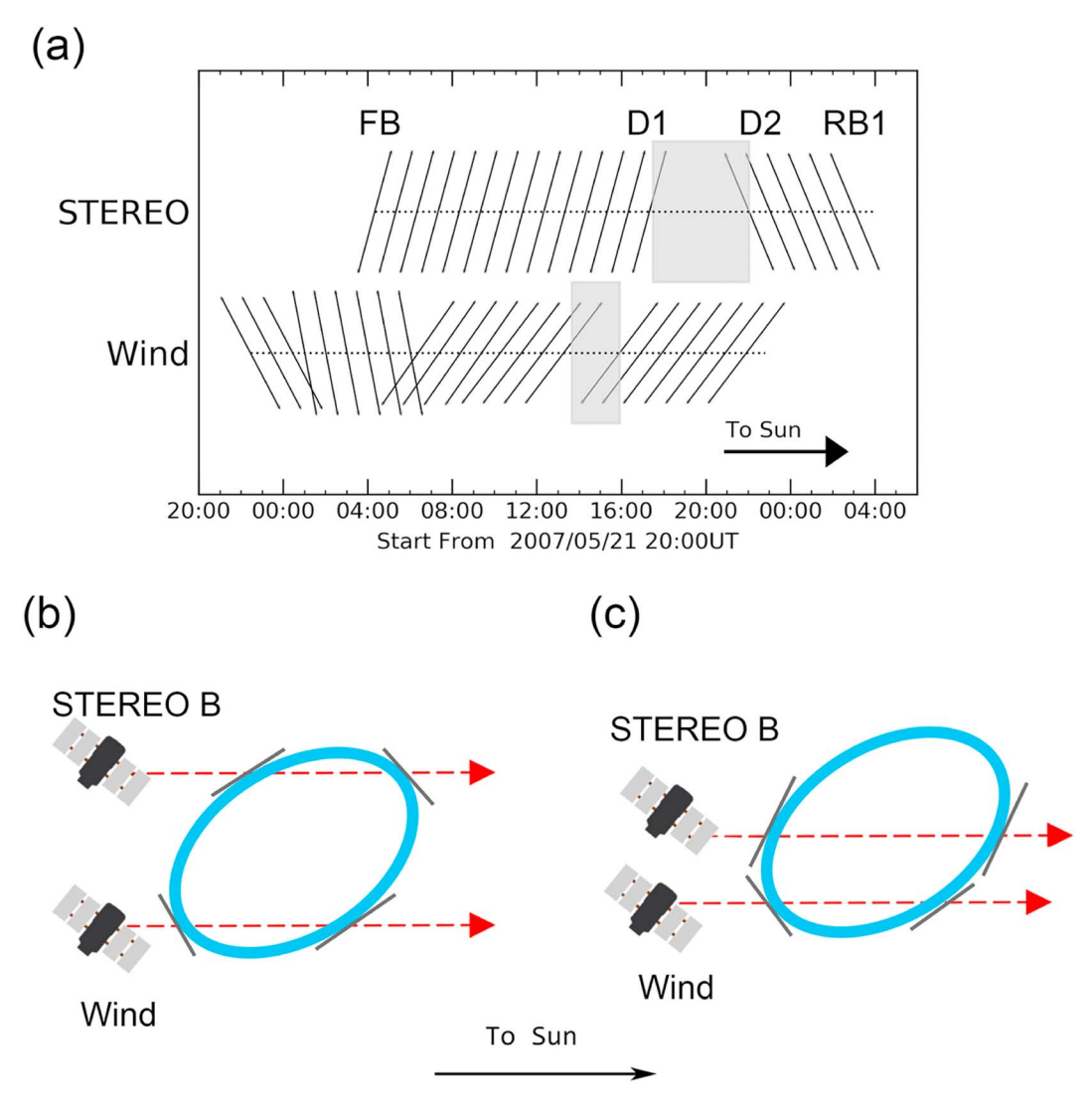


Figure 12. (a) Sketch of the variations of common TDs projected on the ecliptic plane. The gray area represents the location of the high pressure/density region, and the horizontal dotted line indicates the spacecraft trajectory. (b) Sketch of the spacecraft passages across the internal TD (blue circle) when RB1 is the rear boundary of MC. The black line indicates the tangent plane of the TD at the spacecraft position. (c) The case with the D1 or D2 as the rear boundary.

5. Discussion

We have identified five major shock/discontinuity structures observed by both STEREO B and Wind space-craft. They are the boundaries of the MC (FB and RB1), the boundaries of the high pressure/density region (D1 and D2) inside the MC, and the rear boundary of the whole structure embedded in the background HCS (RB2). Generally, it is difficult to identify the rear boundary of a MC exactly due to the unclear end time of magnetic field rotation or the unclear signature of the discontinuity. For the studied MC event in 2007 May, previous literatures have different definitions on the rear boundary. Liu et al. (2008) identified the D1 as the MC rear boundary according to the discontinuities in proton density, bulk speed, and magnetic field

Table 5 Calculated Shock Parameters of D1							
Spacecraft	$\widehat{\mathbf{n}}_{SH}$	ε _{SH} (°)	θ B n (°)	n _d /n _u	M_{f}		
STEREO B Wind	(0.83, -0.54, 0.11) (0.97, 0.22, 0.13)	14 28	81 33	1.4 1.1	1.1 1.1		

strength. But Kilpua et al. (2009) determined the rear boundary to be the D2 based on the end of magnetic field rotation. In this study, by supposing that the MC boundaries are TD structures (Feng et al., 2006) and using the feature that the studied MC is inclined and embedded in the HCS, we suggest that the MC rear boundary is RB1 and the interval between RB1 and RB2 is the transition region from the MC body to the background HCS.



Feng, Lin, et al. (2008) and Lin et al. (2009) argued that TDs sometimes are possibly misinterpreted as slow shocks by single-spacecraft measurements. They proposed that such ambiguities can be resolved through comparing the estimated propagating time of a structure between two distinct spacecraft with the in situ observations. From the shock/discontinuity analysis in this study, we find that D2 can be a reverse slow shock with a normal mainly in the y_{GSE} direction or a TD with a normal mainly in the x_{GSE} direction. By combining with the error estimation of propagation time listed in Table 2, we verify that D2 is a TD structure with the normal direction similar to FB, RB1, and D1.

We further calculate the shock parameters of D1 from both STEREO B and Wind measurements. The results are summarized in Table 5, where θ_{Bn} is the angle between shock normal and upstream magnetic field and M_f is the fast Mach number at the upstream region. The $M_f > 1$ together with the in-phase changes in the magnetic field and plasma density across the D1, as shown in Figure 5, characterize that D1 is a fast shock structure. In addition, we find that D1 is a quasi-perpendicular shock with $\theta_{Bn} = 81^\circ$ when passing through the STEREO B spacecraft but it is a quasi-parallel shock with $\theta_{Bn} = 33^\circ$ encountered by Wind. It is also confirmed by the magnetic field variations presented in Figure 5 that an overshoot behind the ramp is observed at STEREO B corresponding to the signature of quasi-perpendicular shock. On the other hand, more turbulent fields at both upstream and downstream regions observed by Wind are consistent with the feature of a quasi-parallel shock.

Kilpua et al. (2009) indicated that the solar source of this MC event was associated with a prominence eruption. When a whole bunch of material moved outward from the Sun and propagated in the interplanetary space, the interaction between prominence material and ambient plasma may produce the D1 observed both by STEREO B and Wind. After D1 formed, the high pressure/density region developed in the downstream of D1. This region may undergo an expansion and hence triggered D2 behind the shocked expansion region. However, the expansion only induced a TD instead of a shock. Our speculation can be confirmed by the similar normal direction of D1 and D2 since the direction of expansion is supposed to be roughly parallel in two sides of the expansion. In addition, the local magnetic field structures can cause the pressure inhomogeneity, resulting in the different pressure profiles at STEREO B and Wind.

According to the assumption that MC consists of multiple TDs surrounding the MC axis, we attempt to deduce the general picture of the MC field morphology along the spacecraft trajectories directly from the in situ observations of two spacecraft by arbitrarily selecting internal TDs and tracing their B_n / \mid **B** | variations. Although we cannot reconstruct the large-scale magnetic field configurations on the MC cross section and determine the cross-section shape, our results are comparable with the previous results derived from GS reconstruction. As illustrated in Figure 12, the internal TDs at STEREO B almost have the same orientation before the high pressure/density region. One possible interpretation is that STEREO B passed through the MC central area if it encountered the MC rear boundary before the high pressure/density region. It is qualitatively consistent with the GS reconstruction results presented in Liu et al. (2008; see Figure 5), Kilpua et al. (2009; see Figures 1 and 6), and Möstl, Farrugia, Miklenic, et al. (2009; see Figure 4) by imposing the period of FB and D1 or the period of FB and D2 to the reconstruction. However, any approach of estimating the MC magnetic field topology strongly depends on the selected boundaries. In this study, for example, if the MC rear boundary is determined to be at RB1, we propose the other possibility that STEREO B transited the MC region away from the central area based on the hill variation pattern of our common TDs.

6. Conclusions

Using the in situ observations of STEREO B and Wind, the shock/discontinuity analysis is implemented to the MC event during 21–23 May 2007 in this study. Both spacecraft encountered five major discontinuities, that is, FB, D1, D2, RB1, and RB2. Owing to the large inclination of the MC axis to the ecliptic plane, we suggest that the MC boundaries (FB and RB1), which are recognized as TDs, can be distinguished from the ambient regions by showing the background solar wind happens to be a HCS lying on the ecliptic plane. The D1 and D2 are the structures associated with the high pressure/density region embedded in the MC. Based on further examination of the propagation times between two spacecraft, we conclude that D1 is a forward fast shock but D2 is a TD that resembles a reverse slow shock. We also provide different methods to evaluate the uncertainties of normal directions of TDs and shocks. In addition, we estimate the local magnetic field morphology on the MC cross section at spacecraft locations by analyzing the orientations of TDs inside the MC. Based on the



different variation patterns of TD orientations at STEREO B and Wind, it is supposed that these two spacecraft transited the different parts of MC. Moreover, we propose two possibilities of STEREO B passage through the MC depending on the MC rear boundary near or after the high pressure/density region.

Appendix A: Error Cone Angle for Shock Normal

In this study, we obtain the shock normal direction $\widehat{\mathbf{n}}_{SH}$ from the averaged magnetic fields in the upstream and downstream regions based on the coplanarity theorem (Colburn & Sonett, 1966). The corresponding field fluctuations are used to derive the uncertainty of shock normal estimation, which is expressed as the error cone angle ϵ_{SH} .

The size of the error cone is derived based on the concept of Monte-Carlo calculation method. We first select 10 successive data points on each side of a shock covering the interval of magnetic field fluctuations. The variation of shock normal direction $\tilde{\mathbf{n}}_{SH}$ due to field fluctuations is then evaluated via the following equation:

$$\widetilde{\mathbf{n}}_{\mathsf{SH}} = \frac{\left(\widetilde{\mathbf{B}}_{\mathbf{u}}(i) \times \widetilde{\mathbf{B}}_{\mathbf{d}}(j)\right) \times \left(\widetilde{\mathbf{B}}_{\mathbf{u}}(i) - \widetilde{\mathbf{B}}_{\mathbf{d}}(j)\right)}{\left|\left(\widetilde{\mathbf{B}}_{\mathbf{u}}(i) \times \widetilde{\mathbf{B}}_{\mathbf{d}}(j)\right) \times \left(\widetilde{\mathbf{B}}_{\mathbf{u}}(i) - \widetilde{\mathbf{B}}_{\mathbf{d}}(j)\right)\right|},\tag{A1}$$

where $\widetilde{\mathbf{B}}_{\mathbf{u}}$ refers to the magnetic field data array selected in the upstream region with the data point index i = 1, 2, ..., 10 and $\widetilde{\mathbf{B}}_{\mathbf{d}}$ is the downstream field array with the data point index j = 1, 2, ..., 10. Therefore, we have 100 possibilities for the shock normal variation, as represented by the angle between $\widetilde{\mathbf{n}}_{SH}$ and $\widehat{\mathbf{n}}_{SH}$.

$$\phi_{k} = \cos^{-1}(\widetilde{\mathbf{n}}_{SH} \cdot \widehat{\mathbf{n}}_{SH}) \tag{A2}$$

where k = 1, 2, ..., 100. Suppose that the size of the error cone should contain the ϕk distribution with a possibility 0.95. As a result, the error cone angle ϵ_{SH} is evaluated via:

$$\varepsilon_{\text{SH}} = 2\sigma_{\text{d}} = 2\sqrt{\frac{\Sigma_{k=1}^{N}(\varphi_{k}-0)^{2}}{N}}$$
 (A3)

where N is the amount of total data points in this time interval and σ_d is the standard deviation of ϕk with respect to the estimated shock normal direction (i.e., $\phi_k = 0^\circ$).

There are also other methods, for instant, by combining the magnetic field and plasma parameters, to derive the shock normal directions and errors (e.g., Abraham-Shrauner, 1972; Lepping & Argentiero, 1971; Lin et al., 2006). The method provided here will result in a relatively large uncertainty; namely, we may overestimate the size of error cone ε_{SH} .

Appendix B: Error Cone Angle for TD Normal

Based on the property that no normal component of magnetic field across the TD surface, a well-defined TD should have very small amount of the normal component for a sufficient time interval. In this study, we propose that the accuracy of a TD normal estimation can be determined from the amount of the magnetic field deviation from the TD normal direction within a certain time interval, as presented by

$$\omega_{t} = \sin^{-1}\left(\frac{B_{n}}{|\mathbf{B}|}\right),\tag{B1}$$

where B_n and $|\mathbf{B}|$ indicate the magnetic field normal component and strength, respectively. Subscript t represent the data indices within the chosen time interval. Considering the MHD length scale, a 5-min window with the analyzed TD at the central time is used for ω_t calculation.

Since the size of the error corn is supposed to contain the ω_t distribution with a possibility 0.95, the error cone angle ϵ_{SH} is evaluated by

$$\epsilon_{TD} = 2\sigma_d = 2\sqrt{\frac{\Sigma_{t=1}^N(\omega_t - 0)^2}{N}}, \tag{B2}$$

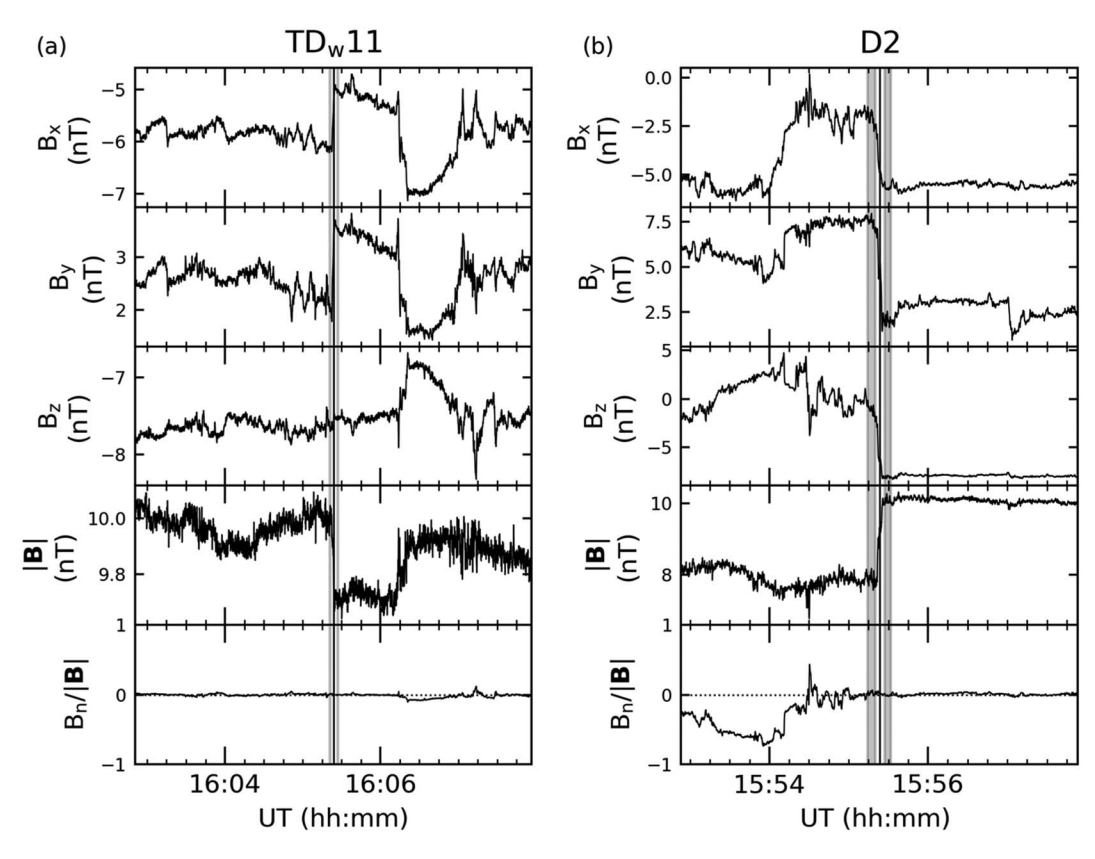


Figure B1. (a) TD_W11 observation from Wind. Panels from top to bottom presents the magnetic field components in GSE coordinate $(B_X, B_y, \text{ and } B_Z)$, magnetic field strength $(|\mathbf{B}|)$, and the time variations of $B_n/|\mathbf{B}|$. The vertical line indicates the transition time of the TD_W11 and the gray regions denote the time interval of side 1 (side 2) for TD normal calculation. (b) D2 observation from Wind with the same format as (a).

where N is the amount of total data points in this time interval and σ_d stands for the degree of deviation relative to the normal direction (i.e., $\omega_t = 0^\circ$). We would like to mention that the errors caused by the small-scale perturbations on the TD surface is not considered in this study.

Figure B1a shows the detail plots of the TD_W11 , where the gray areas indicate the magnetic field data used for TD normal estimation. The projected magnetic fields on this normal, B_n , divided by the magnetic field strength, $|\mathbf{B}|$, are shown in the last Small value of $B_n/|\mathbf{B}|$ implies that the uncertainty of the derived TD normal is small. During the 5 min around the TD_W11 , there is no noticeable MHD disturbances observed. However, when there are cases large variations across the discontinuities, large variation of B_n can occur. Figure B1b shows the detail plots of the D2 from Wind's observation. The error cone of this discontinuity is much bigger than the other TDs. It is due to a large change before time 14:55 UT. The realistic error cone for D2 should be much less than 31.6°.

Acknowledgments

The authors thank NASA/GSFC for providing the data sets of STEREO and Wind, which are available from the Coordinated Data Analysis Web (http://cdaweb.gsfc.nasa.gov/cdaweb/istp_public/) and the Wind Spacecraft website (https://wind.nasa.gov/mfi_swe_plot.php). This work is supported by the Ministry of Science and Technology of the R.O.C. under grants MOST 106-2111-M-008-025 and MOST 107-2111-M-008-014.

References

Abraham-Shrauner, B. (1972). Determination of magnetohydrodynamic shock normals. *Journal of Geophysical Research*, 77(4), 736–739. https://doi.org/10.1029/ia077i004n00736

Al-Haddad, N., Nieves-Chinchilla, T., Savani, N. P., Möstl, C., Marubashi, K., Hidalgo, M. A., et al. (2013). Magnetic field configuration models and reconstruction methods for interplanetary coronal mass ejections. *Solar Physics*, 284(1), 129–149. https://doi.org/10.1007/s11207-013-0244-5

Bothmer, V., & Schwenn, R. (1998). The structure and origin of magnetic clouds in the solar wind. *Annales Geophysicae*, 16(1), 1–24. https://doi.org/10.1007/s005850050575

Burlaga, L. F. (1988). Magnetic clouds and force-free fields with constant alpha. *Journal of Geophysical Research*, 93(A7), 7217. https://doi.org/10.1029/ja093ia07p07217

Burlaga, L. F., Lepping, R. P., & Jones, J. A. (1990). Global configuration of a magnetic cloud. In C. T. Russell, E. R. Rriest, & L. C. Lee (Eds.), *Physics of magnetic flux ropes, Geophysical Monograph Series* (Vol. 58, pp. 373–377). Washington, DC: American Geophysical Union. https://doi.org/10.1029/gm058p0373



- Burlaga, L. F., Ness, N. F., Richardson, J. D., & Lepping, R. P. (2001). The Bastille Day shock and merged interaction region at 63 AU: Voyager 2 observations. Solar Physics, 204(1/2), 399–411. https://doi.org/10.1023/a:1014269926730
- Burlaga, L. F., Sittler, E., Mariani, F., & Schwenn, R. (1981). Magnetic loop behind an interplanetary shock: Voyager, Helios, and IMP 8 observations. *Journal of Geophysical Research: Space Physics*, 86(A8), 6673–6684. https://doi.org/10.1029/ja086ia08p06673
- Chollet, E. E., Mewaldt, R. A., Cummings, A. C., Gosling, J. T., Haggerty, D. K., Hu, Q., et al. (2010). Multipoint connectivity analysis of the May 2007 solar energetic particle events. *Journal of Geophysical Research*, 115, A12106. https://doi.org/10.1029/2010JA015552
- Colburn, D. S., & Sonett, C. P. (1966). Discontinuities in the solar wind. Space Science Reviews, 5(4), 439–506. https://doi.org/10.1007/BF00240575
- Collier, M. R., Lepping, R. P., & Berdichevsky, D. B. (2007). A statistical study of interplanetary shocks and pressure pulses internal to magnetic clouds. *Journal of Geophysical Research*, 112, A06102. https://doi.org/10.1029/2006JA011714
- Crooker, N. U., Burton, M. E., Siscoe, G. L., Kahler, S. W., Gosling, J. T., & Smith, E. J. (1996). Solar wind streamer belt structure. *Journal of Geophysical Research*, 101(A11), 24,331–24,341. https://doi.org/10.1029/96ja02412
- Crooker, N. U., & Intriligator, D. S. (1996). A magnetic cloud as a distended flux rope occlusion in the heliospheric current sheet. *Journal of Geophysical Research*, 101(A11), 24,343–24,348. https://doi.org/10.1029/96ja02129
- Démoulin, P., Dasso, S., & Janvier, M. (2013). Does spacecraft trajectory strongly affect detection of magnetic clouds? *Astronomy & Astrophysics*, 550, A3. https://doi.org/10.1051/0004-6361/201220535
- Du, D., Wang, C., & Hu, Q. (2007). Propagation and evolution of a magnetic cloud from ACE to Ulysses. *Journal of Geophysical Research*, 112, A09101. https://doi.org/10.1029/2007JA012482
- Farrugia, C. J., Berdichevsky, D. B., Möstl, C., Galvin, A. B., Leitner, M., Popecki, M. A., et al. (2011). Multiple, distant (40°) in situ observations of a magnetic cloud and a corotating interaction region complex. *Journal of Atmospheric and Solar-Terrestrial Physics*, 73(10), 1254–1269. https://doi.org/10.1016/j.jastp.2010.09.011
- Farrugia, C. J., Osherovich, V. A., & Burlaga, L. F. (1995). Magnetic flux rope versus the spheromak as models for interplanetary magnetic clouds. *Journal of Geophysical Research*, 100(A7), 12,293–12,306. https://doi.org/10.1029/95ja00272
- Feng, H. Q., Lin, C. C., Chao, J. K., Wu, D. J., Lyu, L. H., & Lee, L. C. (2008). Observations of a switch-off shock in interplanetary space. *Journal of Geophysical Research*, 113, A05216. https://doi.org/10.1029/2007JA012864
- Feng, H. Q., Wu, D. J., & Chao, J. K. (2006). Identification of configuration and boundaries of interplanetary magnetic clouds. *Journal of Geophysical Research*, 111, A07S90. https://doi.org/10.1029/2005JA011509
- Feng, H. Q., Wu, D. J., & Chao, J. K. (2007). Size and energy distributions of interplanetary magnetic flux ropes. *Journal of Geophysical Research*, 112, A02102. https://doi.org/10.1029/2006ja011962
- Feng, H. Q., Wu, D. J., Lin, C. C., Chao, J. K., Lee, L. C., & Lyu, L. H. (2008). Interplanetary small-and intermediate-sized magnetic flux ropes during 1995–2005. *Journal of Geophysical Research*, 113, A12105. https://doi.org/10.1029/2008JA013103
- Galvin, A. B., Kistler, L. M., Popecki, M. A., Farrugia, C. J., Simunac, K. D. C., Ellis, L., et al. (2008). The Plasma and Suprathermal Ion Composition (PLASTIC) investigation on the STEREO observatories. *Space Science Reviews*, 136(1–4), 437–486. https://doi.org/10.1007/s11214-007-
- Goldstein, H. (1983). On the field configuration in magnetic clouds. In M. Neugebauer (Ed.), *Solar wind five* (Vol. 2280, pp. 731–733). Washington, DC: NASA conference publication.
- Good, S. W., Forsyth, R. J., Raines, J. M., Gershman, D. J., Slavin, J. A., & Zurbuchen, T. H. (2015). Radial evolution of a magnetic cloud: MESSENGER, STEREO, and Venus express observations. *The Astrophysical Journal*, 807(2), 177. https://doi.org/10.1088/0004-637x/807/2/177
- Gosling, J. T., Baker, D. N., Bame, S. J., Feldman, W. C., Zwickl, R. D., & Smith, E. J. (1987). Bidirectional solar wind electron heat flux events. Journal of Geophysical Research. 92(A8), 8519. https://doi.org/10.1029/ia092ia08p08519
- Gosling, J. T., Hildner, E., MacQueen, R. M., Munro, R. H., Poland, A. I., & Ross, C. L. (1975). Direct observations of a flare related coronal and solar wind disturbance. Solar Physics, 40(2), 439–448. https://doi.org/10.1007/BF00162390
- Hidalgo, M. A. (2002). A non-force-free approach to the topology of magnetic clouds in the solar wind. *Journal of Geophysical Research*, 107(A1), 1002. https://doi.org/10.1029/2001JA900100
- Hidalgo, M. A. (2013). A global magnetic topology model for magnetic clouds. II. *The Astrophysical Journal*, 766(2), 125. https://doi.org/10.1088/0004-637x/766/2/125
- Hollweg, J. V. (1982). Surface waves on solar wind tangential discontinuities. *Journal of Geophysical Research*, 87(A10), 8065–8076. https://doi.org/10.1029/ja087ia10p08065
- Hu, Q., & Sonnerup, B. U. (2002). Reconstruction of magnetic clouds in the solar wind: Orientations and configurations. *Journal of Geophysical Research*. 107(A7), 1142. https://doi.org/10.1029/2001JA000293
- Jian, L. K., Russell, C. T., Luhmann, J. G., Skoug, R. M., & Steinberg, J. T. (2008). Stream interactions and interplanetary coronal mass ejections at 5.3 AU near the solar ecliptic plane. Solar Physics 250, 250, 375–402. https://doi.org/10.1007/s11207-008-9204-x
- Kaiser, M. L., Kucera, T. A., Davila, J. M., Cyr, O. S., Guhathakurta, M., & Christian, E. (2008). The STEREO mission: An introduction. Space Science Reviews, 136(1–4), 5–16. https://doi.org/10.1007/s11214-007-9277-0
- Kilpua, E., Koskinen, H. E. J., & Pulkkinen, T. I. (2017). Coronal mass ejections and their sheath regions in interplanetary space. Living Reviews in Solar Physics, 14(1). https://doi.org/10.1007/s41116-017-0009-6
- Kilpua, E. K. J., Jian, L. K., Li, Y., Luhmann, J. G., & Russell, C. T. (2011). Multipoint ICME encounters: Pre-STEREO and STEREO observations. Journal of Atmospheric and Solar-Terrestrial Physics, 73(10), 1228–1241. https://doi.org/10.1016/j.jastp.2010.10.012
- Kilpua, E. K. J., Liewer, P. C., Farrugia, C., Luhmann, J. G., Möstl, C., Li, Y., et al. (2009). Multispacecraft observations of magnetic clouds and their solar origins between 19 and 23 May 2007. Solar Physics, 254(2), 325–344. https://doi.org/10.1007/s11207-008-9300-y
- Knetter, T., Neubauer, F. M., Horbury, T., & Balogh, A. (2004). Four-point discontinuity observations using Cluster magnetic field data: A statistical survey. *Journal of Geophysical Research*, 109, A06102. https://doi.org/10.1029/2003JA010099
- Leitner, M., Farrugia, C. J., Möstl, C., Ogilvie, K. W., Galvin, A. B., Schwenn, R., & Biernat, H. K. (2007). Consequences of the force-free model of magnetic clouds for their heliospheric evolution. *Journal of Geophysical Research*, 112, A06113. https://doi.org/10.1029/2006JA011940
- Lepping, R. P., Acūna, M. H., Burlaga, L. F., Farrell, W. M., Slavin, J. A., Schatten, K. H., et al. (1995). The WIND magnetic field investigation. Space Science Reviews, 71(1–4), 207–229. https://doi.org/10.1007/bf00751330
- Lepping, R. P., & Argentiero, P. D. (1971). Single spacecraft method of estimating shock normals. *Journal of Geophysical Research*, 76(19), 4349–4359. https://doi.org/10.1029/ja076i019p04349
- Lepping, R. P., Berdichevsky, D. B., Wu, C. C., Szabo, A., Narock, T., Mariani, F., et al. (2006). A summary of WIND magnetic clouds for years 1995–2003: Model-fitted parameters, associated errors and classifications. *Annales Geophysicae*, 24(1), 215–245. https://doi.org/10.5194/angeo-24-215-2006



- Lepping, R. P., Jones, J. A., & Burlaga, L. F. (1990). Magnetic field structure of interplanetary magnetic clouds at 1 AU. *Journal of Geophysical Research*. 95(A8). 11.957–11.965. https://doi.org/10.1029/ja095ja08p11957
- Lin, C. C., Chao, J. K., Lee, L. C., Lyu, L. H., & Wu, D. J. (2006). A new shock fitting procedure for the MHD Rankine-Hugoniot relations for the case of small He2+slippage. *Journal of Geophysical Research*, 111, A09104. https://doi.org/10.1029/2005JA011449
- Lin, C. C., Feng, H. Q., Wu, D. J., Chao, J. K., Lee, L. C., & Lyu, L. H. (2009). Two-spacecraft observations of an interplanetary slow shock. *Journal of Geophysical Research*, 114, A03105. https://doi.org/10.1029/2008JA013154
- Liu, Y., Luhmann, J. G., Huttunen, K. E. J., Lin, R. P., Bale, S. D., Russell, C. T., & Galvin, A. B. (2008). Reconstruction of the 2007 May 22 magnetic cloud: How much can we trust the flux-rope geometry of CMEs? *The Astrophysical Journal*, 677(2), L133–L136. https://doi.org/10.1086/587830
- Liu, Y., Richardson, J. D., Belcher, J. W., Wang, C., Hu, Q., & Kasper, J. C. (2006). Constraints on the global structure of magnetic clouds: Transverse size and curvature. *Journal of Geophysical Research*, 111, A12S03. https://doi.org/10.1029/2006JA011890
- Luhmann, J. G., Curtis, D. W., Schroeder, P., McCauley, J., Lin, R. P., Larson, D. E., et al. (2008). STEREO IMPACT investigation goals, measurements, and data products overview. Space Science Reviews, 136(1–4), 117–184. https://doi.org/10.1007/978-0-387-09649-0_6
- Moldwin, M., Ford, S., Lepping, R., Slavin, J., & Szabo, A. (2000). Small-scale magnetic flux ropes in the solar wind. *Geophysical Research Letters*, 27(1), 57–60. https://doi.org/10.1029/1999GL010724
- Möstl, C., Farrugia, C. J., Biernat, H. K., Leitner, M., Kilpua, E. K. J., Galvin, A. B., & Luhmann, J. G. (2009). Optimized grad-Shafranov reconstruction of a magnetic cloud using STEREO-Wind observations. *Solar Physics*, 256(1–2), 427–441. https://doi.org/10.1007/s11207-009-9360-7
- Möstl, C., Farrugia, C. J., Kilpua, E. K. J., Jian, L. K., Liu, Y., Eastwood, J. P., et al. (2012). Multi-point shock and flux rope analysis of multiple interplanetary coronal mass ejections around 2010 August 1 in the inner heliosphere. *The Astrophysical Journal*, 758, 10. https://doi.org/10.1088/0004-637X/758/1/10
- Möstl, C., Farrugia, C. J., Miklenic, C., Temmer, M., Galvin, A. B., Luhmann, J. G., et al. (2009). Multispacecraft recovery of a magnetic cloud and its origin from magnetic reconnection on the Sun. *Journal of Geophysical Research*, 114, A04102. https://doi.org/10.1029/2008JA013657
- Mulligan, T., & Russell, C. T. (2001). Multispacecraft modeling of the flux rope structure of interplanetary coronal mass ejections: Cylindrically symmetric versus nonsymmetric topologies. *Journal of Geophysical Research*, 106(A6), 10,581–10,596. https://doi.org/10.1029/2000ja900170
- Nakwacki, M. S., Dasso, S., Démoulin, P., Mandrini, C. H., & Gulisano, A. M. (2011). Dynamical evolution of a magnetic cloud from the Sun to 5.4 AU. Astronomy & Astrophysics, 535(A52). https://doi.org/10.1051/0004-6361/201015853
- Ogilvie, K. W., Chornay, D. J., Fritzenreiter, R. J., Hunsaker, F., Keller, J., Lobell, J., et al. (1995). SWE, a comprehensive plasma instrument for the Wind spacecraft. Space Science Reviews, 71(1-4), 55–77. https://doi.org/10.1007/bf00751326
- Owens, M. J. (2006). Magnetic cloud distortion resulting from propagation through a structured solar wind: Models and observations. *Journal of Geophysical Research*, 111, A12109. https://doi.org/10.1029/2006JA011903
- Richardson, J. D., Dashevskiy, F., & Paularena, K. I. (1998). Solar wind plasma correlations between L1 and Earth. *Journal of Geophysical Research*, 103(A7), 14,619–14,629. https://doi.org/10.1029/98JA00675
- Richardson, J. D., Liu, Y., Wang, C., & Burlaga, L. F. (2006). ICMES at very large distances. Advances in Space Research, 38(3), 528–534. https://doi.org/10.1016/j.asr.2005.06.049
- Riley, P., Linker, J. A., Lionello, R., Mikić, Z., Odstrcil, D., Hidalgo, M. A., et al. (2004). Fitting flux ropes to a global MHD solution: A comparison of techniques. *Journal of Atmospheric and Solar-Terrestrial Physics*, 66(15–16), 1321–1331. https://doi.org/10.1016/j.jastp.2004.03.019
- Riley, P., Linker, J. A., Mikić, Z., Odstrcil, D., Zurbuchen, T. H., Lario, D., & Lepping, R. P. (2003). Using an MHD simulation to interpret the global context of a coronal mass ejection observed by two spacecraft. *Journal of Geophysical Research*, 108(A7), 1272. https://doi.org/10.1029/
- Rodriguez, L., Zhukov, A. N., Dasso, S., Mandrini, C. H., Cremades, H., Cid, C., et al. (2008). Magnetic clouds seen at different locations in the heliosphere. *Annales Geophysicae*, 26(2), 213–229. https://doi.org/10.5194/angeo-26-213-2008
- Rouillard, A. P. (2011). Relating white light and in situ observations of coronal mass ejections: A review. *Journal of Atmospheric and Solar-Terrestrial Physics*, 73(10), 1201–1213. https://doi.org/10.1016/j.jastp.2010.08.015
- Ruffenach, A., Lavraud, B., Owens, M. J., Sauvaud, J. A., Savani, N. P., Rouillard, A. P., et al. (2012). Multispacecraft observation of magnetic cloud erosion by magnetic reconnection during propagation. *Journal of Geophysical Research*, 117, A09101. https://doi.org/10.1029/2012ia017624
- Sheeley, N. R. Jr., Michels, D. J., Howard, R. A., & Koomen, M. J. (1980). Initial observations with the Solwind coronagraph. *The Astrophysical Journal*, 237, L99–L101. https://doi.org/10.1086/183243
- Skoug, R. M., Feldman, W. C., Gosling, J. T., McComas, D. J., Reisenfeld, D. B., Smith, C. W., et al. (2000). Radial variation of solar wind electrons inside a magnetic cloud observed at 1 and 5 AU. *Journal of Geophysical Research*, 105(A12), 27,269–27,275. https://doi.org/10.1029/2000ja000095
- Tsurutani, B. T., & Gonzalez, W. D. (1997). The interplanetary causes of magnetic storms: A review. In B. T. Tsurutani, W. D. Gonzalez, Y. Kamide, & J. K. Arballo (Eds.), Magnetic storms, Geophysical Monograph Series (Vol. 98, pp. 77–89). Washington, DC: American Geophysical Union.
- Von Steiger, R., & Richardson, J. D. (2006). ICMEs in the outer heliosphere and at high latitudes: An introduction. *Coronal Mass Ejections*, 111–126. https://doi.org/10.1007/978-0-387-45088-9_8
- Wang, Y., Shen, C., Liu, R., Liu, J., Guo, J., Li, X., et al. (2018). Understanding the twist distribution inside magnetic flux ropes by anatomizing an interplanetary magnetic cloud. *Journal of Geophysical Research: Space Physics*, 123, 3238–3261. https://doi.org/10.1002/2017ja024971
- Wang, Y., Zhou, Z., Shen, C., Liu, R., & Wang, S. (2015). Investigating plasma motion of magnetic clouds at 1 AU through a velocity-modified cylindrical force-free flux rope model. *Journal of Geophysical Research: Space Physics, 120*, 1543–1565. https://doi.org/10.1002/2014ja020494Yu
- Wang, Y. M., Ye, P. Z., Wang, S., & Xue, X. H. (2003). An interplanetary cause of large geomagnetic storms: Fast forward shock overtaking preceding magnetic cloud. *Geophysical Research Letters*, 30(13), 1700. https://doi.org/10.1029/2002GL016861
- Wei, F., Liu, R., Fan, Q., & Feng, X. (2003). Identification of the magnetic cloud boundary layers. *Journal of Geophysical Research*, 108(A6), 1263. https://doi.org/10.1029/2002JA009511
- Yu, W., Farrugia, C. J., Lugaz, N., Galvin, A. B., Kilpua, J. E. K., Kucharek, H., et al. (2014). A statistical analysis of properties of small transients in the solar wind 2007–2009: STEREO and Wind observations. *Journal of Geophysical Research: Space Physics*, 119, 689–708. https://doi.org/10.1002/2013JA019115